NATIONAL ADVISORY COMMITTEE FOR AERONAUTICS

TECHNICAL NOTE 2646

INVISCID FLOW ABOUT AIRFOILS AT HIGH SUPERSONIC SPEEDS

By A. J. Eggers, Jr., and Clarence A. Syvertson

Ames Aeronautical Laboratory
Moffett Field, Calif.

Washington
March 1952

NATIONAL ADVISORY COMMITTEE FOR AERONAUTICS

TECHNICAL NOTE 2646

INVISCID FLOW ABOUT AIRFOILS AT HIGH SUPERSONIC SPEEDS

By A. J. Eggers, Jr., and Clarence A. Syvertson

SUMMARY

Steady flow about curved airfoils is investigated analytically at high supersonic speeds. Assuming air behaves as an ideal diatomic gas, it is found that small pressure disturbances emanating from the surface of an airfoil are almost completely absorbed in the leading-edge shock wave (or a shock wave emanating from any other location on the surface), provided the flow deflection angles are not too close to those corresponding to shock detachment. This result is found to be essentially independent of Mach number. As a consequence, it is shown that within the limitations of the assumption of ideal gas flow, the shock-expansion method may be used with good accuracy to predict pressure distributions on curved airfoils at arbitrarily high Mach numbers. This observation is verified with the aid of the method of characteristics applied to a 10-percent-thick biconvex airfoil at 0° angle of attack. It is further shown that the shock-expansion method can be easily employed to construct the entire flow field about a curved airfoil, accounting for shock-wave curvature and resulting entropy gradients in the flow.

An approximation to the shock-expansion method for thin airfoils at high Mach numbers is also investigated, and is found to yield pressure distributions in error by less than 10 percent at Mach numbers above 3 and flow deflection angles up to 25°. This slender-airfoil method is relatively simple in form and thus may prove useful for some engineering purposes. To this end, tables are presented to facilitate its use.

Effects of caloric imperfections of air manifest in disturbed flow fields at high Mach numbers are investigated, particular attention being given to the reduction of the ratio of specific heats from 1.4 toward 1.0. So long as this ratio does not decrease appreciably below 1.3, it is indicated that the shock-expansion method, generalized to include effects of these imperfections, should be substantially as accurate as for ideal gas flows. This point is checked by comparing pressure distributions predicted by the generalized shock-expansion method and a generalized method of characteristics. Both methods are employed in forms

applicable for local air temperatures up to about 5000° Rankine, corresponding, for slender airfoils, to Mach numbers up to the order of the so-called escape Mach number. Caloric imperfections caused reductions in the pressure coefficients below those predicted for flows of an ideal gas. In turn, there is a general reduction in force and moment coefficients up to 10 percent.

The slender-airfoil method is modified to employ an average value of the ratio of specific heats for a particular flow field. This simplified method has essentially the same accuracy for imperfect gas flows as its counterpart has for ideal gas flows.

An approximate flow analysis is made at extremely high Mach numbers where it is indicated that the ratio of specific heats may approach close to 1. It is found that the shock-expansion method may be in considerable error as disturbances incident on the leading-edge shock wave are no longer largely absorbed in the wave. In this case, however, the Busemann method for the limit of infinite free-stream Mach number and specific heat ratio of 1 appears to apply with reasonable accuracy.

INTRODUCTION

Small-disturbance, potential-flow theories have been employed widely, and for the most part successfully, for predicting the pressures (and velocities) at the surface of an airfoil in steady motion at low supersonic speeds. Thus the linear theory of Ackeret (reference 1) has proven particularly useful in studying the flow about relatively thin, sharp-nosed airfoils at small angles of attack, while the second-order theory of Busemann (reference 2) has found application when thicker airfoils at larger angles of attack were under consideration. At high free-stream Mach numbers the range of applicability of any potential theory is seriously limited, however, due to the production of strong shocks by even the relatively small flow deflections caused by thin airfoils. The assumption of potential flow is invalidated, of course, by the pronounced entropy rises occurring through these shocks.

This limitation on potential theories was early recognized and led to the adoption (see reference 3) of what is now commonly called the shock-expansion method. The latter method derives its advantage over potential theories principally by accounting for the entropy rise through the oblique shock emanating from the leading edge of a sharp-nosed airfoil. Consequently, so long as the disturbed air behaves essentially like an ideal gas, and so long as entropy gradients normal to the streamlines (due to curvature of the surface) do not significantly influence flow at the surface, the shock-expansion theory should predict the pressures at the surface of an airfoil with good accuracy -

it is tacitly assumed, of course, that the flow velocity is everywhere supersonic, and that the Reynolds number of the flow is sufficiently large to minimize viscous effects on surface pressures.

The departure of the behavior of air from that of an ideal gas at the temperatures encountered in flight at high supersonic speeds has been the subject of some investigation in the case of flows through oblique shock waves. In reference 4, the effects of thermal and caloric imperfections on the pressure rise across an oblique shock wave was investigated at sea-level Mach numbers of 10 and 20 and it was found that these effects decreased the rise by less than 5 percent for maximum temperatures up to 3000° R (corresponding to flow deflection angles up to 24°). This decrease was found to be due almost entirely to caloric imperfections or changes in vibrational heat capacities of the air passing through the shock wave. The changes in temperature and density of the air passing through the wave were affected to a considerably greater extent. Subsequently, an investigation was carried out by Ivey and Cline up to Mach numbers as high as 100 (reference 5) using the results for normal shock waves obtained by Bethe and Teller considering effects of dissociation (reference 6). As would be expected, the pressures were found to be affected to a somewhat greater extent at the higher Mach numbers.

The extent to which flow in the region of the leading edge of an airfoil departs from the simple Prandtl-Meyer type has also been investigated at high supersonic airspeeds. If the surface is curved, for example, to give an expanding flow downstream of the leading edge, expansion waves from the surface will interact with the nose shock wave, thereby curving it and yielding a nonisentropic flow field. This flow field may be characterized not only by disturbances emanating from the surface but also by disturbances reflecting to some extent from the shock wave back toward the surface. The manner in which these phenomena dictate shock-wave curvature and surface pressure gradient in ideal gas flows at the leading edge has been treated by Crocco (reference 7) and more recently by Schaefer (reference 8), Munk and Prim (reference 9), and others. In the cases considered by Munk and Prim it was found that surface pressure gradients were less (in absolute value) than those obtained assuming Prandtl-Meyer flow at the higher Mach numbers (i.e., Mach numbers greater than about 3) although generally by no more than about 10 percent. Since curved airfoils are likely to be of fundamental interest at high flight speeds (see, e.g., reference 10), these phenomena would appear to merit further investigation, particularly as regards their influence on the whole flow field. In addition it would appear desirable to consider effects of gaseous imperfections throughout the field.

Such an investigation has therefore been undertaken in the present report using the method of characteristics to accurately obtain flow fields, and as a basis for obtaining the more approximate methods of analysis. The method is employed in a generalized form which allows caloric imperfections as well as entropy gradients in the flow to be considered at temperatures up to the order of 5000° R - thermal imperfections are neglected as being unimportant in atmospheric air flows (see reference 4). A 10-percent-thick biconvex airfoil is treated at Mach numbers from 3.5 to infinity, and the results are compared with the predictions of the shock-expansion method, including a simplified form of the method applicable to slender airfoils at high Mach numbers, and a generalized form of the method including effects of caloric imperfections.

SYMBOLS

a	local speed of sound, feet per second
c	chord, feet
C_1, C_2	characteristic coordinates (C_1 positively inclined and C_2 negatively inclined with respect to the local velocity vector)
C_d	section drag coefficient
C_l	section lift coefficient
C_m	section moment coefficient (moment taken about leading edge)
C_p	pressure coefficient $\left(\frac{p - p_o}{q_o}\right)$
c_p	specific heat at constant pressure, foot-pounds per slug °R
c_v	specific heat at constant volume, foot-pounds per slug °R
M	Mach number (ratio of local velocity to local speed of sound)
p	static pressure, pounds per square foot
q	dynamic pressure, pounds per square foot
R	gas constant, foot-pounds per slug °R

s,n	rectangular coordinates (in streamline direction and normal to streamline direction, respectively)
T	temperature, ^{o}R
t	time, seconds
V	resultant velocity, feet per second
x,y	rectangular coordinates
α	angle of attack, radians unless otherwise specified
β	Mach angle, arc sine $\left(\frac{1}{M}\right)$, radians
γ	ratio of specific heats $\left(\frac{c_p}{c_v}\right)$ (Average value of γ is γ_a.)
δ	flow deflection angle, radians unless otherwise specified
θ	molecular vibrational energy constant, ^{o}R (5500^{o} R for air)
ρ	mass density, slugs per cubic foot
σ	shock-wave angle, radians
ω	ray angle for Prandtl-Meyer flow, radians

Subscripts

o	free-stream conditions
A,B, C,D...	conditions at different points in flow field
i	ideal gas quantities
N	conditions just downstream of shock wave
S	conditions on streamline

Superscript

-	vector quantities

DEVELOPMENT OF METHODS OF ANALYSIS

Method of Characteristics

Two-dimensional rotational supersonic flows have been treated by numerous authors with the aid of the method of characteristics, and various adaptations of the method have been found which are especially suited for studying particular types of such flows. In the case of steady flows in which atmospheric air does not behave as an ideal diatomic gas, a very familiar and simple form of the compatibility equations may be employed. To illustrate, consider the Euler equation

$$\rho \frac{d\bar{V}}{dt} = - \text{grad } p \tag{1}$$

the continuity equation

$$\text{div } (\rho\bar{V}) = 0 \tag{2}$$

and the equation for the speed of sound (evaluated at constant entropy)

$$a^2 = \frac{dp}{d\rho} \tag{3}$$

Rewriting equations (1) and (2) in the form of partial differential equations and transforming the resulting expressions to the characteristic or C_1, C_2 coordinate system, there is obtained, upon combination with equation (3), the following relations for steady flow:

$$\frac{\text{ctg } \beta}{\rho V^2}\left(\frac{\partial p}{\partial C_1} - \frac{\partial p}{\partial C_2}\right) + \left(\frac{\partial \delta}{\partial C_1} + \frac{\partial \delta}{\partial C_2}\right) = 0 \tag{4}$$

and

$$\frac{\text{ctg } \beta}{\rho V^2}\left(\frac{\partial p}{\partial C_1} + \frac{\partial p}{\partial C_2}\right) + \left(\frac{\partial \delta}{\partial C_1} - \frac{\partial \delta}{\partial C_2}\right) = 0 \tag{5}$$

A simple addition or subtraction of equations (4) and (5) then yields the compatibility equations (see, e.g., reference 11)

$$\frac{\partial p}{\partial C_1} = - \rho V^2 \tan \beta \frac{\partial \delta}{\partial C_1} \tag{6}$$

and

$$\frac{\partial p}{\partial C_2} = \rho V^2 \tan \beta \frac{\partial \delta}{\partial C_2} \tag{7}$$

Now, in reference 4 both caloric and thermal imperfections of air were considered and it was found that the latter imperfections[1] have a negligible effect on shock processes in atmospheric air. It may easily be shown that this conclusion also applies to expansion processes, and for this reason caloric imperfections, only, are considered in detail in the present paper. These imperfections become significant in air at temperatures greater than about 800° R and first manifest themselves as changes in the vibrational heat capacities with temperature. Thus, the specific heats, c_p and c_v, and their ratio, γ, for the gas also change. The equation of state remains, however,

$$p = \rho RT \tag{8}$$

and the specific heats are still related to the gas constant by the expression

$$c_p - c_v = R \tag{9}$$

Furthermore, it readily follows from the differential energy equation and these expressions that the speed of sound is given by the simple relation

$$a^2 = \gamma RT \tag{10}$$

Combining equations (8) and (10) and noting that $\sin \beta = a/V$ there is then obtained

$$\rho V^2 = \frac{\gamma p}{\sin^2 \beta} \tag{11}$$

Hence, on combining this equation with equations (6) and (7), it is apparent that the familiar compatibility equations

$$\frac{\partial p}{\partial C_1} = \frac{-2\gamma p}{\sin 2\beta} \frac{\partial \delta}{\partial C_1} \tag{12}$$

[1]Thermal imperfections usually appear in the form of intermolecular forces and molecular-size effects, and may be accounted for with additional terms in the equation of state.

and

$$\frac{\partial p}{\partial C_2} = \frac{2\gamma p}{\sin 2\beta} \frac{\partial \delta}{\partial C_2} \tag{13}$$

also hold for the more general type of flow under consideration. These equations are basic, of course, to two-dimensional characteristics theory, and, as will be shown later, form a convenient starting point for developing simpler theories of two-dimensional supersonic flow.

In order to apply equations (12) and (13), it is evident that the manner in which γ and β or M are connected to p or δ must be known. Relations implicitly connecting these variables at temperatures up to the order of 5000° R may be readily obtained from the results of reference 4 by simply eliminating the terms therein accounting for thermal imperfections. Thus we have as a function of the local static temperature and free-stream conditions

$$\gamma = \gamma_i \left[\frac{1 + \left(\frac{\gamma_i - 1}{\gamma_i}\right) \left(\frac{\theta}{T}\right)^2 \frac{e^{\theta/T}}{(e^{\theta/T} - 1)^2}}{1 + (\gamma_i - 1) \left(\frac{\theta}{T}\right)^2 \frac{e^{\theta/T}}{(e^{\theta/T} - 1)^2}} \right] \tag{14}$$

and

$$M^2 = \frac{2}{\gamma} \left(\frac{T_o}{T}\right) \left[\frac{\gamma_o M_o^2}{2} + \frac{\gamma_i}{\gamma_i - 1} \left(1 - \frac{T}{T_o}\right) + \frac{\theta}{T_o} \left(\frac{1}{e^{\theta/T_o} - 1} - \frac{1}{e^{\theta/T} - 1} \right) \right] \tag{15}$$

For isentropic flow along a streamline, the pressure is related to the temperature by the expression

$$\frac{p}{p_N} = \frac{\psi(T_N)}{\psi(T)} \tag{16}$$

where

$$\psi(T) = \frac{e^{\theta/T} - 1}{e^{\left(\frac{\theta}{T} \frac{e^{\theta/T}}{e^{\theta/T} - 1}\right)}} \left(\frac{1}{T}\right)^{\frac{\gamma_i}{\gamma_i - 1}} \tag{17}$$

If there is a shock wave in the flow,[2] in particular a nose or leading-edge shock, then the following additional relations obtained with equations (8), (10), and (15) and the conditions for continuity of flow and conservation of momentum along a streamline through the shock are also required:

$$\frac{p_o}{p_N} = \frac{1}{2}\left\{ (1+\gamma_N M_N^2) - \frac{T_o}{T_N}(1+\gamma_o M_o^2) + \sqrt{\left[(1+\gamma_N M_N^2) - \frac{T_o}{T_N}(1+\gamma_o M_o^2)\right]^2 + 4\frac{T_o}{T_N}} \right\} \tag{18}$$

$$\sin^2\sigma = \frac{\dfrac{\gamma_N T_N M_N^2}{\gamma_o T_o M_o^2} - 1}{\left(\dfrac{\rho_o}{\rho_N}\right)^2 - 1} \tag{19}$$

and

$$\tan\delta = \frac{1}{\tan\sigma}\,\frac{1}{\dfrac{\gamma_o M_o^2}{(p_N/p_o)-1} - 1} \tag{20}$$

Using the local static temperature as a parameter, the term $2\gamma p/\sin 2\beta$ in equations (12) and (13) may now be evaluated with equations (14) through (17). Equations (18) through (20) define the initial conditions downstream of a leading-edge or other shock wave in the flow field. Thus, equations (12) through (20) provide all the information necessary to calculate the flow about an airfoil by means of the method of characteristics. As described in detail in appendix A, the calculation is of three general types; namely, (1) calculation of conditions at a point in the flow field between the shock and the surface; (2) calculation of conditions at a point on the surface; and (3) calculation of conditions at a point just downstream of the shock. Case (1) entails the use of both compatibility equations, while case (2) entails the use of the compatibility equation for a second-family characteristic

[2] If there are no shock waves, then the subscript N in equation (16) can, of course, be replaced with the subscript o.

line in combination with the equation of the airfoil surface, and case (3) involves the compatibility equation for a first-family line in combination with the oblique shock equations. With the aid of the three general types of calculations the entire flow field about an airfoil can be built up numerically using a computing procedure working from the leading edge downstream. In cases where changes in the vibrational heat capacities with temperature are neglected, the calculations are of course simplified since γ of the gas can be considered constant, and temperature, pressure, and density ratios are simply the ideal gas functions of Mach number.

Shock-Expansion Method

General.- This method of calculating supersonic flow of an ideal gas at the surface of an airfoil is well known, entailing simply the calculation of flow at the nose with the oblique shock equations and flow downstream of the nose with the Prandtl-Meyer equations. Determination of airfoil characteristics in this manner requires a small amount of time, of course, compared to that involved when the method of characteristics is used, hence the advantage of the former method. The questions arise, however, as to exactly what the simplifying assumptions underlying the shock-expansion method are, and what form the method takes (for calculative purposes) when the gas displays varying vibrational heat capacities.

The matter of simplifying assumptions may perhaps best be considered by employing equations (12) and (13), the basic compatibility equations. If these expressions are resolved into the streamline direction and combined, noting that

$$\frac{\partial p}{\partial s} = \frac{1}{2 \cos \beta}\left(\frac{\partial p}{\partial C_1} + \frac{\partial p}{\partial C_2}\right) \tag{21}$$

and

$$\frac{\partial \delta}{\partial s} = \frac{1}{2 \cos \beta}\left(\frac{\partial \delta}{\partial C_1} + \frac{\partial \delta}{\partial C_2}\right) \tag{22}$$

there is then obtained the relation

$$\frac{\partial p}{\partial s} = \left(\frac{1 - \dfrac{\partial \delta / \partial C_1}{\partial \delta / \partial C_2}}{1 + \dfrac{\partial \delta / \partial C_1}{\partial \delta / \partial C_2}}\right) \frac{2 \gamma p}{\sin 2 \beta} \frac{\partial \delta}{\partial s} \tag{23}$$

defining the gradient of p along s. If flow along streamlines downstream of the nose is of the simple Prandtl-Meyer type, however, we have

$$\frac{\partial p}{\partial s} = \frac{2\gamma p}{\sin 2\beta} \frac{\partial \delta}{\partial s} \tag{24}$$

Hence it is evident that the requirement for this type of flow is

$$\left| \frac{\partial \delta / \partial C_1}{\partial \delta / \partial C_2} \right| << 1 \tag{25}$$

Equation (25) is, of course, simply an approximate statement of a well-known property of Prandtl-Meyer flows; namely, that flow inclination angles are essentially constant along first-family Mach lines. It follows from equation (12) that if equation (25) holds, then the pressures will also be essentially constant along these lines. It does not follow, however, that the Mach number will be constant, or for that matter that the first-family characteristic lines will be straight (as is the case for isentropic expansion flows about a corner). In fact, it may easily be shown that the Mach number gradient along C_1 is proportional to the local entropy gradient normal to the streamlines, and that the C_1 lines are curved according to the change in M. Thus we see that there is really only one basic assumption underlying the shock-expansion method; namely, disturbances incident on the nose shock (or for that matter any other shock) are consumed almost entirely in changing the direction of the shock.[3] Within the limitations of this assumption it is evident that the method provides a relatively simple means for calculating the whole flow field about an airfoil, including effects of shock-wave curvature (see appendix B). In general, of course, the validity of this assumption can only be checked by comparison of calculations using this method with those using the method of characteristics.

The shock-expansion method for a calorically imperfect diatomic gas is readily deduced from the equations previously obtained. For example, flow conditions at the leading edge of an airfoil can be evaluated with the oblique shock-wave expressions (equations (18) through (20)) and the expression for conservation of energy (equation (15)). The variation of flow inclination angle with pressure along the surface is then

[3]It is interesting to note that the assumption of Thomas (reference 12) that pressure is a function only of flow deflection angle and entropy is equivalent to this assumption. It follows, of course, that the most general solution obtainable with Thomas's series representation of the pressure is that given by the shock-expansion method.

obtained by graphically integrating equation (24); namely,

$$\delta_S - \delta_N = \int_{p_S}^{p_N} \frac{\sin 2\beta}{2\gamma p}\, dp \tag{26}$$

where the variables γ, p, and β are evaluated using equations (14) through (17), employing the static temperature as a parameter. When extreme accuracy is not essential, this rather tedious calculation can be avoided and a relatively simple algebraic solution of the flow downstream of the nose can be employed.[4] The details of this solution are presented in appendix C. In the special case of flow at high supersonic speeds about slender airfoils, the whole calculation becomes particularly simple and warrants special attention.

Slender airfoils.- If it is assumed that the local surface slopes are small compared to 1 and in addition that the free-stream Mach number is large compared to 1, it follows that σ and β are everywhere small compared to 1. In this case equation (24) takes on the approximate form

$$\left.\frac{dp}{d\delta}\right|_S = \gamma p M \tag{27}$$

Furthermore, if it is assumed that γ is constant at an average value γ_a for a particular flow field (this assumption appears reasonable since in the temperature range up to 5000° R the change in γ is less than 10 percent as shown in reference 4), then the Mach number and pressure may be related by the simple expression

$$M = M_N \left(\frac{p_N}{p}\right)^{\frac{\gamma_a - 1}{2\gamma_a}} \tag{28}$$

Equations (27) and (28) combine to yield the differential equation

$$\frac{1}{\gamma_a M_N} \left(\frac{p}{p_N}\right)^{-\frac{(\gamma_a+1)}{2\gamma_a}} d\left(\frac{p}{p_N}\right) = d\delta \tag{29}$$

which readily integrates (between N and S) to the form

[4] The tabulated results of Noyes (reference 13) may also prove useful in this case for Mach numbers up to 3.

$$\frac{p_S}{p_N} = \left[1 - \left(\frac{\gamma_a - 1}{2} M_N \delta_N \right) \left(1 - \frac{\delta_S}{\delta_N} \right) \right]^{\frac{2\gamma_a}{\gamma_a - 1}} \tag{30}$$

Now denoting

$$\frac{\gamma_a - 1}{2} M_N \delta_N = f(M_o \delta_N) \tag{31}$$

and

$$\frac{p_N}{p_o} = g(M_o \delta_N) \tag{32}$$

there is obtained from the oblique shock equations, simplified to conform with this analysis,

$$f(M_o \delta_N) = \frac{M_o^2 \sigma_N^2 - 1}{\sqrt{\left(M_o^2 \sigma_N^2 + \frac{2}{\gamma_a - 1} \right) \left(\frac{2\gamma_a}{\gamma_a - 1} M_o^2 \sigma_N^2 - 1 \right)}} \tag{33}$$

and

$$g(M_o \delta_N) = \frac{2\gamma_a M_o^2 \sigma_N^2 - (\gamma_a - 1)}{\gamma_a + 1} \tag{34}$$

where

$$M_o \sigma_N = \frac{\gamma_a + 1}{4} M_o \delta_N + \sqrt{1 + \left(\frac{\gamma_a + 1}{4} M_o \delta_N \right)^2} \tag{35}$$

With equations (30) through (35) the pressures on the surface of an airfoil may easily be obtained. In terms of pressure coefficient we have

$$C_p = \frac{2}{\gamma_a M_o^2} \left[\left(\frac{p_N}{p_o} \right) \left(\frac{p_S}{p_N} \right) - 1 \right] \tag{36}$$

or

$$C_p = \frac{2}{\gamma_a M_o^2} \left\{ g(M_o \delta_N) \left[1 - f(M_o \delta_N) \left(1 - \frac{\delta_S}{\delta_N} \right) \right]^{\frac{2\gamma_a}{\gamma_a - 1}} - 1 \right\} \tag{37}$$

The advantage of these slender-airfoil expressions lies, of course, in their relative simplicity and thus the ease of calculation which is inherent to them. It may be noted in this regard that the functions $f(M_o\delta_N)$ and $g(M_o\delta_N)$ can be calculated once and for all with equations (33), (34), and (35), provided the variation of γ_a with $M_o\delta_N$ is known. This calculation has been carried out for a constant value of γ equal to 1.4, and average values of γ assuming $T_o = 500^\circ$ R.[5] The results are presented in table I.

It should also be noted that the slender-airfoil expressions of the shock-expansion method satisfy the hypersonic similarity law for airfoils first deduced by Tsien (reference 14).[6] A necessary condition for the validity of these expressions is thus satisfied; however, the accuracy of the shock-expansion method, whether for slender airfoils or otherwise, remains to be investigated. Such an investigation is now undertaken with the aid of the method of characteristics.

INVESTIGATION OF FLOW ABOUT AIRFOILS AND DISCUSSION OF RESULTS

This study is divided into two parts: first, a consideration of the effects of Mach number assuming air behaves as an ideal diatomic gas; and second, a consideration of the combined effects of Mach number and gaseous imperfections, with principal emphasis in the latter regard placed on the caloric imperfections previously discussed.

Ideal Gas Flows

The effects of Mach number of primary interest here are, of course, those which result from interaction between the leading-edge (or other) shock wave and small disturbances originating on the surface of an airfoil. Some insight into the nature and extent of these effects can be obtained in the region just downstream of the shock wave without regard

---

[5]For a given value of T_o, T_N, to the accuracy of this analysis, is the ideal gas function of $M_o\delta_N$. Thus, knowing T_N, γ_N can be determined. The average value of γ used is $\gamma_a = \gamma_a(M_o\delta_N) = \frac{\gamma_N+\gamma_i}{2}$.

[6]This fact was employed by Linnell (reference 15) to obtain an expression for pressure coefficient equivalent to equation (37) for the case of constant γ, and to obtain explicit solutions for the lift, drag, and pitching-moment coefficients of several airfoils at hypersonic speeds.

for the shape of the airfoil producing the shock. To this end it is convenient to consider the ratio $\frac{\partial\delta/\partial C_1}{\partial\delta/\partial C_2} = -\frac{\partial p/\partial C_1}{\partial p/\partial C_2}$ (see equation (25)) which may be termed "the disturbance strength ratio" since in the region under consideration it is a measure of the ratio of strengths of disturbances reflected from the shock wave to disturbances incident on the wave. This ratio may be evaluated with the expression

$$\frac{\partial\delta/\partial C_1}{\partial\delta/\partial C_2} = \frac{\left(\frac{2\gamma_N p_N}{\sin 2\beta_N} - \left.\frac{dp}{d\delta}\right|_N\right)}{\left(\frac{2\gamma_N p_N}{\sin 2\beta_N} + \left.\frac{dp}{d\delta}\right|_N\right)} \frac{\sin(\beta_N + \delta_N - \sigma)}{\sin(\beta_N - \delta_N + \sigma)} \tag{38}$$

which is easily obtained with the compatibility equations and the oblique shock-wave equations as shown in appendix D. This calculation has been carried out for Mach numbers from 3.5 to ∞ ($\gamma_N = 1.4$) and flow deflection angles approaching those corresponding to shock detachment (i.e., $M_N \approx 1$) and the results are presented in figure 1. It is evident that except near $M_N \approx 1$, the ratio is small (in absolute value) compared to 1 throughout the entire range considered - this observation also applies, of course, at lower supersonic Mach numbers. Thus it is indicated that almost all of an incident disturbance is generally absorbed in the shock wave, provided the air behaves like an ideal diatomic gas.[7] This result is substantially the same, of course, as that which is assumed in deriving the shock-expansion method of calculating flows about airfoils, and therefore yields some credence in the method for high Mach number as well as low Mach number applications.

As an over-all check on the shock-expansion method, surface pressure distributions calculated thereby are compared in figure 2 with those obtained with the method of characteristics for a 10-percent-thick biconvex airfoil ($\alpha = 0^\circ$) operating at free-stream Mach numbers of 3.5, 5, 7.5, 10, 15, and ∞. Predictions of the slender-airfoil approximation to the former method for high supersonic speeds are also shown. There is no apparent difference between the pressure distributions given by the method of characteristics and the shock-expansion method up to a

[7]This result is contrary to that obtained by Lighthill (reference 16) who reports that for hypersonic flows, a disturbance is reflected from a shock wave with opposite sign but essentially undiminished strength. Lighthill's conclusion appears to be based on an incorrect evaluation of his results for the case of very high Mach numbers.

Mach number of 10. At Mach numbers of 10, and above, however, the latter method predicts pressures which are slightly low downstream of the nose, becoming progressively lower with increasing Mach number. This result would be deduced from figure 1 where it is observed that, at the Mach numbers under consideration, expansion waves incident on the nose shock are reflected back toward the surface as compression waves of relatively small but increasing strength with increasing Mach number. The effect of these waves does not become pronounced even at infinite Mach number (see fig. 2(f)) and the shock-expansion method is thus substantiated as being a reliable simplified method for predicting the flow about airfoils at high supersonic speeds, again, so long as the air behaves as an ideal diatomic gas. The further simplified slender-airfoil method also appears to be a good approximation over the entire range of Mach numbers,[8] although, as would be expected from the assumptions made in its development, it is in somewhat greater error than the shock-expansion method at the lower Mach numbers.

The relative accuracy at high Mach numbers of the slender-airfoil method, linear and second-order potential theories may be seen in figure 3. As might be expected, the slender-airfoil method is more accurate than linear theory at both $M_o = 5$ and 15, and more accurate than second-order theory at $M_o = 15$. It is perhaps surprising to note, however, that at the lower Mach number of 5 the slender-airfoil method is also somewhat superior to the second-order theory.

The pressure distributions of figures 2 and 3 have been employed to calculate the zero-lift drag of the biconvex airfoil, and the results of these calculations, along with additional predictions of linear and second-order theory, are shown in figure 4. Predictions of the shock-expansion method are, of course, in best agreement with those of the method of characteristics; while the slender-airfoil method, although slightly less accurate than the shock-expansion method, is apparently superior to both linear and second-order theory at Mach numbers above 3.

The preceding findings verify that so long as the disturbance strength ratio is small compared to 1, the flow along streamlines is essentially of the Prandtl-Meyer type. If we choose, on the basis of these findings, a maximum absolute value for $\frac{\partial\delta/\partial c_1}{\partial\delta/\partial c_2}$ of 0.06 (note the maximum value of $\frac{\partial\delta/\partial c_1}{\partial\delta/\partial c_2}$ for the cases presented in fig. 2 was

[8]The hybrid expression for pressure coefficient obtained by Ivey and Cline (reference 5) gives reasonably good results also, although not as accurate as the slender-airfoil method at the higher Mach numbers under consideration.

approximately 0.06 at $M_0 = \infty$), the region in which the shock-expansion method is applicable can readily be obtained from figure 1. The upper boundary line of this region is shown in figure 5 and it is evident that it lies only slightly below (about 1° in general) the line corresponding to shock detachment given approximately by the $M_N = 1.0$ line. Almost the entire region of completely supersonic (ideal gas) flow is then covered by the method.[9] (See shaded area of fig. 5.)

The question naturally arises concerning the corresponding range of applicability of the slender-airfoil method. This question may be answered in part by comparing separately the predictions of the method for oblique shock flows and expansion flows with those of the exact oblique shock equations and Prandtl-Meyer equations. Such a comparison is shown in figure 6 in terms of the percentage error in the pressure coefficients predicted by the slender-airfoil method. As would be expected, this method does not exhibit good accuracy over the wide range of applicability of the shock-expansion method; however, it is indicated that it should predict pressure coefficients with less than 10-percent error down to Mach numbers as low as 3 for airfoils producing flow deflections up to as high as 25°.

As a further check on the utility of the slender-airfoil method, the pressure coefficients on the 10-percent-thick biconvex airfoil have been calculated with this method and the shock-expansion method at a Mach number of 10 and angles of attack up to about 30°.[10] The results of this calculation are shown in figure 7 (see fig. 2(d) for $\alpha = 0^\circ$) where it is seen that the agreement is reasonably good even at the highest angle of attack. This fact is reflected in figure 8 showing the force and moment coefficients for the airfoil as a function of angle of attack. Little difference is observed in the force coefficients as calculated by the two methods, while the moment coefficients display more pronounced but nevertheless small differences at the higher angles of attack.

---

[9]If it is required as by Rand (reference 17) that the entire flow field be of the true Prandtl-Meyer type (i.e., that all flow properties be constant along first-family Mach lines and not just δ and p), then the range of applicability of the shock-expansion method would be appreciably smaller. However, it has been shown that this restriction is not necessary.

[10]These conditions are within the range of applicability of the shock-expansion method as defined in figure 4; hence the use of the method as a base of comparison seems justified. Since the shock-expansion method is far less tedious to apply than the method of characteristics, it will be employed as such a base in subsequent calculations whenever the conditions being investigated have been determined to be within its range of applicability.

From these and previous considerations, the ranges of applicability of the shock-expansion and slender-airfoil methods for ideal supersonic gas flows are reasonably well established. It remains now to determine the manner and extent to which gaseous imperfections in the flow at higher supersonic speeds may alter these ranges, and the reasons therefor.

Imperfect Gas Flows

As a first step toward investigating the effects of gaseous imperfections on the high Mach number flows under consideration, it is convenient to extend our consideration of the disturbance strength ratio $\frac{\partial\delta/\partial c_1}{\partial\delta/\partial c_2}$. It is recalled that when air exhibits a constant value of γ equal to 1.4 (the value for an ideal diatomic gas), the disturbance strength ratio is small at arbitrarily large Mach numbers, provided the flow deflection angles are not too close to those for shock detachment. One of the most important effects of gaseous imperfections is, however, to decrease γ of the disturbed air below this value due to the excitation of additional degrees of freedom (e.g., vibrational) in the molecules at the high temperatures encountered at high Mach numbers. Indeed, at arbitrarily high Mach numbers it might be expected that γ of the disturbed air would approach 1, since the number of degrees of freedom may effectively become very large (see, e.g., references 3 and 6). In this case, however, the extent of the disturbance flow field is decreased to a layer at the surface of the body which is negligibly thin compared to that for the case of ideal gas flow. Thus it is apparent that significant changes in the flow about airfoils at high Mach numbers may result from decreases in γ of the disturbed air; hence the effects of such decreases on the disturbance strength ratio would appear to warrant attention.

A detailed analysis of these effects is impractical at the present time due to the limited range over which the variation of γ with temperature is known. However, some knowledge of these effects can be gained by repeating the ideal gas calculations for constant values of γ_N between 1.4 and 1.0.[11] Such calculations have been carried out at

[11]Since the enthalpy is negligibly small compared to the mass kinetic energy of the undisturbed fluid at the high Mach numbers of interest and, hence, γ of this fluid does not influence the flow, this approach corresponds to employing an average value of γ for the disturbed fluid. Since only flows of dense air are considered here, heat-capacity-lag phenomena are neglected (see references 5 and 6).

infinite Mach number since in this case $\frac{\partial\delta/\partial C_1}{\partial\delta/\partial C_2}$ has its maximum value for a given γ_N, and the results are presented in figure 9. It is seen that except near shock detachment, the disturbance strength ratio increases with decreasing γ_N, approaching 1 as γ_N approaches 1. This increase is slow at first; for example, the value of $\frac{\partial\delta/\partial C_1}{\partial\delta/\partial C_2}$ is still less than 0.1 at $\gamma_N = 1.3$. It might therefore be expected that the shock-expansion method would continue to apply with reasonable accuracy so long as γ of the disturbed flow is not appreciably less than this value. This point has been checked with the methods developed previously for analyzing the flow of a calorically imperfect diatomic gas at local air temperatures up to about 5000° R (note γ has a value only slightly less than 1.3 at this temperature). In particular, the pressure distribution on the lower surface of the biconvex airfoil at $M_o = 10$, $\alpha=19.9^\circ$, and $T_o = 500^\circ$ R ($T_N \approx 4000^\circ$ R at leading edge) has been calculated with both the method of characteristics and the shock-expansion method.[12] The results of these calculations are presented in figure 10 and it would appear that the conclusions drawn from figure 9 pertaining to cases where γ_N is of the order of 1.3 or greater are substantiated. Pressures in the expansion flow about the upper surface are not influenced (due to the low temperatures) by caloric imperfections and hence are the same as shown in figure 7(b).

Shown also in figure 10 is the pressure distribution obtained by the shock-expansion method for an ideal gas ($\gamma_i = 1.4$). It is apparent, on comparing this pressure distribution with the other distributions, that although the effect of caloric imperfections on the disturbance strength ratio is small, the pressures are appreciably reduced by the increase in specific heats. The extent of this reduction is more completely illustrated in figure 11 where the lower surface pressure distributions on the biconvex airfoil are presented for $M_o=10$ and $T_o=500^\circ$ R, at $\alpha = 0^\circ$, 10°, 19.9°, and 30°. As one might expect, the reduction in pressures increases with angle of attack (due to the corresponding increase in static temperature of the disturbed air). The pressure coefficients calculated with consideration for the imperfections in the gas are less on the lower surface (up to 6 percent at the leading edge and 15 percent at the trailing edge) than those calculated assuming the gas behaves ideally. The upper-surface pressures are again unaffected

[12]For added ease of calculation the expansion method of appendix C was employed. This method is also employed in all subsequent calculations of this type since it has been found to yield results differing by less than 1 percent from those obtained by the more tedious graphical integration method.

by the caloric imperfections of air in all the cases presented (except at $\alpha = 0^\circ$) since this surface experiences lower pressures and hence lower temperatures. They are therefore the same as shown in figure 7. Shown also in figure 11 are the pressure distributions calculated with the slender-airfoil method for $\gamma = \gamma_a$. The accuracy of this simplified method is substantially the same as was previously observed for the corresponding method in the case of ideal gas flows, although the local error may be greater than the reduction in pressure coefficients due to the caloric imperfections of air. This error is somewhat compensating, however, in its effects on the force and moment coefficients, as will be seen.

The force and moment coefficients, corresponding to the lower-surface pressure distributions shown in figure 11 and the upper-surface distributions of figure 7 are presented in figure 12. The reduction in the lower-surface pressures leads, of course, to a general reduction in all three coefficients (up to about 10 percent for $\alpha = 30^\circ$). The slender-airfoil method again predicts these coefficients with surprising accuracy.

In order to further assess the accuracy of the slender-airfoil method some additional calculations were carried out for the biconvex airfoil at $\alpha = 0^\circ$ and $M_0 = 20$ and 30. The pressure distributions for these cases were calculated by the shock-expansion method, slender-airfoil method ($\gamma = \gamma_a$), and slender-airfoil method ($\gamma = \gamma_i$). These results are presented in figure 13 and it is observed that the use of γ_a rather than γ_i improves the accuracy of the slender-airfoil method. The extent of this improvement in the case of drag coefficient is shown in figure 14 - it would appear that predictions of the slender-airfoil method ($\gamma = \gamma_a$) and shock-expansion method are in as good agreement as for ideal gas flows (see fig. 4). On the basis of these and previous results, it may be concluded then that not only does the shock-expansion method retain its range of applicability when air exhibits caloric imperfections provided γ of the disturbed air is not appreciably less than 1.3, but also the slender-airfoil method ($\gamma = \gamma_a$) retains its range.

It would be surprising indeed, however, if this conclusion continued to apply as γ of the disturbed fluid approached 1 since, as discussed previously, $\dfrac{\partial\delta/\partial C_l}{\partial\delta/\partial C_{\ell}}$ is not small compared to 1 in this case, but would appear, in fact, to approach 1. This matter may be investigated in the same manner as the effect of γ_N on the disturbance strength ratio was investigated, namely, by using the ideal gas relationships in combination with appropriate values of γ.

The limiting case of infinite free-stream Mach number and $\gamma = 1.0$ (for the disturbed fluid, see footnote 11) has already been investigated by Busemann (reference 18) and more recently by Ivey, Klunker, and Bowen (reference 19). In this case, as pointed out previously, the shock wave emanating from the leading edge remains attached to the surface downstream of the leading edge (this is easily verified with the oblique shock-wave equations) and the disturbance flow field is confined to an infinitesimally thin layer adjacent to the surface. In addition, the velocity along a streamline downstream of the shock is constant, as may easily be shown with the compatibility equations. Surface pressures therefore become a simple function of airfoil geometry,

$$C_p = 2 \sin^2 \delta_S + 2 \cos \delta_S \frac{d\delta_S}{dx} \int_0^x \sin \delta_S dx \qquad (39)$$

varying, to a first approximation, directly with the square of the component of free-stream velocity normal to the surface (i.e., the flow is approximately of the Newtonian corpuscular type). With this theory then, and the method of characteristics, we can get an idea of both the extent to which extreme changes of γ from 1.4 toward 1 will alter surface pressures, and the accuracy with which the shock-expansion theory predicts the alterations. To this end, figure 15 is presented showing the pressure distributions about the biconvex airfoil at $M_0 = \infty$ as calculated by the several methods for different values of γ. It is observed that, whereas the shock-expansion method agrees very closely with the method of characteristics for $\gamma = 1.4$, there is a large difference at $\gamma = 1.05$. This, of course, is precisely what one would expect from the previous discussion of the disturbance strength ratio. On the other hand, if the two characteristic solutions and the Busemann method are considered in order of decreasing γ, it is indicated that the characteristics solutions approach the Busemann theory as γ approaches 1. For $\gamma = 1.0$ and $M_0 = \infty$ the shock-expansion method, in turn, predicts a discontinuous pressure distribution with a pressure coefficient equal to that of the Busemann theory at the leading edge but a pressure coefficient of zero at all points downstream of the leading edge. Hence it may be concluded that when the free-stream Mach number approaches infinity and γ approaches 1, the Busemann method rather than the shock-expansion method for calculating the flow about airfoils should be employed.

CONCLUDING REMARKS

The flow about curved airfoils was investigated analytically at high supersonic speeds first assuming air behaves as an ideal gas, and then assuming air behaves as a thermally, although not necessarily

calorically, perfect gas. (Caloric imperfections had previously been observed to be of predominant importance in free flight, at least for local air temperatures up to the order of 5000° R.) It was found that so long as air exhibits no imperfections (i.e., behaves as an ideal diatomic gas) small disturbances originating on the curved surface of an airfoil are almost completely absorbed in the shock wave emanating from the leading edge (or any other location on the surface), provided the flow deflection angles are not too close to those corresponding to shock detachment. This result is essentially independent of Mach number, and is consistent with the early calculations of Crocco concerning surface pressure gradient at the leading edge of an airfoil. It was concluded that in ideal gas flows the shock-expansion method for determining flow conditions at the surface of an airfoil would apply with good accuracy at arbitrarily high Mach numbers. This conclusion was verified by the excellent agreement found between pressure distributions on a 10-percent-thick biconvex airfoil at 0° angle of attack calculated with the shock-expansion method and the method of characteristics. It was further shown that the former method can be easily employed to construct the entire flow field about an airfoil in a manner that would account for shock-wave curvature and entropy gradients resulting therefrom.

A high Mach number approximation to the shock-expansion method for thin airfoils was also investigated, and was found to apply with good accuracy at Mach numbers above 3 and flow deflection angles up to 25°. The essential feature of this slender-airfoil method is, of course, its simplicity, and for that reason it may prove useful for some engineering purposes.

Effects of caloric imperfections were first investigated qualitatively considering the reduction in the ratio of specific heats from 1.4 toward 1.0. It was found that as the ratio decreased, the extent to which disturbances reflected from a shock wave increased. In the limit as the ratio approached 1, the reflection was complete, and the shock wave became tangent to the surface of the airfoil. So long as the ratio did not decrease appreciably below 1.3, however, it was found that less than 10 percent of a disturbance was reflected; hence the simple shock-expansion method might be expected to continue to apply. This matter was checked quantitatively for the biconvex airfoil with the aid of a generalized method of characteristics including effects of caloric imperfections (up to local air temperatures of the order of 5000° R, corresponding to a ratio of specific heats of about 1.3). It was found that the shock-expansion method was substantially as accurate as for ideal gas flows, provided it was also generalized to include effects of these imperfections. The principal effect of the reduction in specific heat ratio was to reduce the pressure coefficients below their ideal gas values by as much as 15 percent. The reduction in force and moment coefficients was somewhat smaller, being about 10 percent. Similarly it was found that the slender-airfoil method, modified to employ an

average value of the ratio of specific heats for a particular flow field, exhibited essentially the same accuracy as the analogous method for ideal gas flows. Thus it is indicated that the generalized shock-expansion method and its slender-airfoil counterpart can be applied with good accuracy up to very high free-flight Mach numbers. If the flow deflection angles are less than about 12°, these Mach numbers are of the order of the so-called escape Mach number (i.e., Mach numbers as high as 30 to 35).

At even higher Mach numbers where the ratio of specific heats is expected to decrease appreciably below 1.3, and in fact perhaps to approach 1, it was not possible to obtain an accurate check on the previously discussed qualitative considerations. It was undertaken, however, to compare the pressure distributions on the biconvex airfoil predicted by the Busemann method (for the limit of the ratio of specific heats approaching 1 and Mach number approaching infinity) with those predicted by the shock-expansion method and the method of characteristics at infinite Mach number (employing a constant ratio of specific heats of 1.05). As was expected, the shock-expansion method was in very poor agreement with the method of characteristics, whereas the Busemann method was in relatively good agreement. It is therefore indicated that for extremely high Mach numbers (something in excess of the sea-level escape Mach number) the Busemann theory may apply.

Ames Aeronautical Laboratory
National Advisory Committee for Aeronautics
Moffett Field, Calif., Jan. 9, 1952

APPENDIX A

METHOD OF CHARACTERISTICS FOR TWO-DIMENSIONAL FLOW OF A CALORICALLY IMPERFECT GAS

In the application of the method of characteristics for a calorically imperfect diatomic gas to the particular problem of analyzing the flow about curved two-dimensional airfoils, many of the calculations are identical to those encountered in the solution of any problem where characteristics theory is employed. Since the details of these calculations are well known and well reported (see, e.g., reference 11), they will not be repeated here.

A lattice-point system with an initial-value, numerical computing procedure will be used. The form of the compatibility equations to be employed was developed previously;[13] however, it is convenient for purposes of calculation to substitute the pressure ratio, p/q_o, into these equations and to rewrite them as difference equations. Equations (12) and (13) are thus reduced to the following forms

$$(p/q_o)_C - (p/q_o)_A = -\lambda_A(\delta_C - \delta_A) \tag{A1}$$

and

$$(p/q_o)_C - (p/q_o)_B = \lambda_B (\delta_C - \delta_B) \tag{A2}$$

where

$$\lambda = \frac{2\gamma(p/q_o)}{\sin 2\beta} \tag{A3}$$

It is also convenient to employ several reference curves. These curves can be divided into two groups. The general reference curves consist of γ and $\psi(T)$ as a function of temperature, T. Equations (14) and (17) are

[13] This form of the compatibility equations (in p and δ coordinates) was also used in obtaining some of the characteristics solutions for ideal gas flows. The majority of these solutions were carried out, however, with the compatibility equations in β, δ, and entropy coordinates, since it was found that greater accuracy was usually obtained for a given net size. In general, the net size employed yielded pressures at from 30 to 35 surface points on an airfoil with a maximum error in the corresponding pressure coefficients equal to less than 1 percent of the pressure coefficient at the leading edge.

used to determine these curves. A second set of shock-wave reference curves consisting of p/q_o, σ, and δ as a function of temperature, T, are determined by use of equations (18) through (20) - the values of T_o and M_o are presumed known.

In the computations three types of points are encountered. These are (1) a point in the flow field between the shock wave and the airfoil surface, (2) a point on the airfoil surface, and (3) a point just downstream of the shock wave. Each one of these types of points requires a slightly different computing procedure and they will be considered in order.

Point in the Flow Field Between the Shock Wave and the Airfoil Surface

Figure 16(a) shows a schematic diagram of the system of points to be considered in these calculations. Point C is the unknown point at the intersection of the first-family characteristic line passing through point A and the second-family characteristic line passing through point B. Six quantities are known at both points A and B, and the problem is to calculate these same quantities at point C. These quantities are x, y, δ, p/q_o, T, and T_N. The first five quantities are of obvious significance. The sixth, T_N, is defined as the static temperature, just downstream of the shock wave, on the streamline passing through the point C.

The physical coordinates of the point C (x_C, y_C) may be determined by standard procedures such as those given in reference 11. In order to determine the quantity δ_C, it is necessary to solve equations (A1) and (A2) simultaneously; thus

$$\delta_C = \frac{\lambda_A \delta_A + \lambda_B \delta_B + (p/q_o)_A - (p/q_o)_B}{\lambda_A + \lambda_B} \qquad (A4)$$

Equation (A1) or (A2) is then used to obtain $(p/q_o)_C$.

There remains only the problem of determining T_C and T_{N_C} at point C. The temperature T_{N_C} is obviously constant along the streamline through C. This quantity may therefore be calculated in the same manner as the entropy is calculated in similar flow fields for ideal gas processes (see, e.g., reference 11). Furthermore, since the flow along streamlines downstream of the shock wave is isentropic, equation (16) may be applied in the form

$$\frac{(p/q_o)_C}{(p/q_o)_{N_C}} = \frac{\psi(T_{N_C})}{\psi(T_C)} \tag{A5}$$

The pressure, $(p/q_o)_{N_C}$, is defined in a manner analogous to T_{N_C}, and may thus be determined using the shock-wave reference curves and the known value of T_{N_C}. Similarly, $\psi(T_{N_C})$ may be determined from the general reference curves. The only unknown in equation (A5) then is $\psi(T_C)$ which may now be calculated. Once $\psi(T_C)$ is determined, T_C may be determined by again using the general reference curves. All six quantities, x_C, y_C, δ_C, $(p/q_o)_C$, T_C, and T_{N_C} have now been determined.

Point on the Airfoil Surface

Figure 16(b) shows a schematic diagram of the points to be considered in these calculations. The physical coordinates of point C, (x_C, y_C), are first calculated by solving simultaneously the equation of the second-family Mach line passing through point B and the equation of the airfoil surface. When x_C and y_C have been determined, δ_C is readily obtained from the equation of the airfoil surface. Equation (A2) is then applied to determine $(p/q_o)_C$.

Since the airfoil surface is a streamline, T_{N_C} is constant along the surface and may be evaluated at the leading edge. The temperature, T_C, may then be determined using equation (A5) and the previously described procedure. All six quantities, x_C, y_C, $(p/q_o)_C$, δ_C, T_C, and T_{N_C}, are thus determined.

In the special case of the first point on the airfoil surface downstream of the leading edge, the pressure ratio is calculated using the procedure of reference 9. This procedure is easily shown to be applicable to calorically imperfect gas flows providing the oblique shock-wave equations of the present paper are employed.

Point on the Shock Wave

Figure 16(c) shows a schematic diagram of the points to be considered in these calculations. The physical coordinates of point C (x_C, y_C) are first calculated by solving simultaneously the equation

of the first-family Mach line passing through point A and the equation of the shock wave linearized at point D, the last known point on the wave. The variation of p/q_o with δ along the shock wave may be approximated by the relation

$$(p/q_o)_C - (p/q_o)_D = \left.\frac{d(p/q_o)}{d\delta}\right|_N (\delta_C - \delta_D) \qquad (A6)$$

In this equation $\left.\frac{d(p/q_o)}{d\delta}\right|_N$ is the rate of change of p/q_o with δ along the downstream side of the shock wave evaluated at point D. Because of the complicated nature of the shock-wave equations, it is generally easier to evaluate $\left.\frac{d(p/q_o)}{d\delta}\right|_N$ graphically or numerically from the shock-wave reference curves. Equations (A1) and (A6) are solved simultaneously for δ_C, thus

$$\delta_C = \frac{\lambda_A \delta_A + \left.\frac{d(p/q_o)}{d\delta}\right|_N \delta_D + (p/q_o)_A - (p/q_o)_D}{\lambda_A + \left.\frac{d(p/q_o)}{d\delta}\right|_N} \qquad (A7)$$

When δ_C has been calculated, T_C, and in turn $(p/q_o)_C$, may be determined from the shock-wave reference curves. Since point C in this case is just downstream of the shock wave, T_C and T_{N_C} are identical. The six quantities, x_C, y_C, $(p/q_o)_C$, δ_C, T_C, and T_{N_C} have now been determined.

APPENDIX B

SHOCK-EXPANSION METHOD FOR CALCULATING THE FLOW FIELD ABOUT AN AIRFOIL

An initial value procedure which is similar to, although markedly simpler than, that associated with the method of characteristics may be employed to carry out this calculation.[14] To illustrate, consider the sketch:

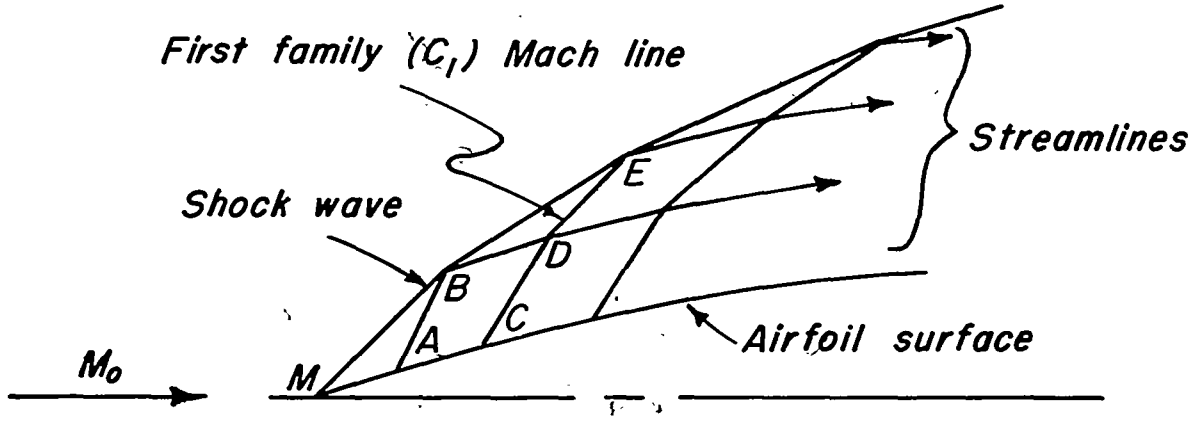

With the oblique shock-wave and expansion equations, all fluid properties at points M, A, C, and so forth on the airfoil surface may be calculated in the usual manner. If the point A is chosen close to M, the first-family (C_1) Mach line connecting A to point B on the shock wave may be considered straight and inclined at an angle to the free-stream direction equal to $\beta_A + \delta_A$. Similarly, the segment MB of the shock wave may be considered straight and inclined at the angle σ_M to the stream direction. Thus the point B in the flow field may easily be determined. The direction of BD (a segment of the streamline passing through B) is the same as the tangent to the surface at A, and the attitude of the segment BE of the shock wave is fixed by this direction. The locations of points D and E in the flow field are thus fixed once point C is chosen.[15] The construction of the remainder of the flow field follows in a similar fashion. Having determined the shapes of the streamlines, the fluid properties along these lines are, of course, determined in the same manner as those along the surface.

---

[14] It is clear, of course, that an "average value" procedure could also be employed. Such a procedure would, in fact, be the more desirable in some cases, since a coarser net may be used.

[15] The point C should, of course, be chosen close to A.

It is important to note that this method is applicable to the determination of the flow not only in the region adjacent to the airfoil (whether the surface be concave or convex) but also in the region downstream of the airfoil; hence it may, for example, prove useful in downwash studies and the like.

APPENDIX C

APPROXIMATE SOLUTION FOR PRANDTL-MEYER FLOW OF A CALORICALLY IMPERFECT GAS

The following solution is obtained with an analysis similar to that used in Meyer's original paper (reference 20). A schematic diagram of the subject flow field is shown in figure 17. It is evident that the change in flow-inclination angle for Prandtl-Meyer flow can be written as follows

$$\delta_N - \delta = (\beta_N - \beta) + (\omega_N - \omega) \tag{C1}$$

Since the flow is isentropic, a given value of the local pressure will determine the Mach angle, β. The problem then is to evaluate the angle, ω. To this end the velocity components tangential and normal to the first-family Mach lines may be expressed in the usual manner in terms of a potential φ, thus

$$u = \frac{\partial \varphi}{\partial r} \tag{C2}$$

$$a = \frac{1}{r}\frac{\partial \varphi}{\partial \omega} \tag{C3}$$

It is clear, however, that these components are functions of ω only; hence it is convenient to define a new velocity potential which is a function of ω alone. Such a potential is

$$\Phi(\omega) = \frac{\varphi}{r} \tag{C4}$$

The velocity components may then be written in terms of this new potential.

$$u = \Phi \tag{C5}$$

$$a = \Phi_\omega \tag{C6}$$

The resultant velocity is given by the expression

$$V^2 = \Phi^2 + \Phi_\omega{}^2 \tag{C7}$$

Equation (15) for conservation of energy may be written in terms of the local temperature as follows:

$$V^2 + 2\left(\frac{\gamma_i}{\gamma_i - 1}\right)RT + 2RT\left(\frac{\theta/T}{e^{\theta/T} - 1}\right) = A^2 \tag{C8}$$

The constant, A, is evaluated at the conditions existing upstream of the expansion region; namely,

$$A^2 = V_N^2 + \left(\frac{2\gamma_i}{\gamma_i - 1}\right)RT_N + 2RT_N\left(\frac{\theta/T_N}{e^{\theta/T_N} - 1}\right) \tag{C9}$$

Equations (C7) and (C8) are then combined to yield

$$\Phi^2 + \Phi_\omega^2 = -2RT\left(\frac{\gamma_i}{\gamma_i - 1} + \frac{\theta/T}{e^{\theta/T} - 1}\right) + A^2 \tag{C10}$$

It was shown previously, however, that

$$a^2 = \gamma RT \tag{C11}$$

Equations (C6), (C10), and (C11) may therefore be combined to obtain the following relationship:

$$\Phi^2 + \Phi_\omega^2\left[1 + \frac{2}{\gamma}\left(\frac{\gamma_i}{\gamma_i - 1} + \frac{\theta/T}{e^{\theta/T} - 1}\right)\right] = A^2 \tag{C12}$$

or

$$\Phi^2 + \Phi_\omega^2\left\{\frac{\gamma_i + 1}{\gamma_i - 1} + \frac{2}{\gamma_i - 1}\left[\frac{\gamma_i}{\gamma} - 1 + \frac{\gamma_i - 1}{\gamma_i}\left(\frac{\gamma_i}{\gamma}\right)\frac{\theta/T}{e^{\theta/T} - 1}\right]\right\} = A^2 \tag{C13}$$

From the imperfect gas relationship for γ we have

$$\frac{\gamma_i}{\gamma} = \frac{1 + (\gamma_i - 1)\left(\frac{\theta}{T}\right)^2 \frac{e^{\theta/T}}{(e^{\theta/T} - 1)^2}}{1 + \left(\frac{\gamma_i - 1}{\gamma_i}\right)\left(\frac{\theta}{T}\right)^2 \frac{e^{\theta/T}}{(e^{\theta/T} - 1)^2}} \tag{C14}$$

Substituting this relation into equation (C13) there is then obtained

$$\Phi^2 + \Phi_\omega{}^2 \left[\frac{\gamma_i+1}{\gamma_i-1} + \frac{2}{\gamma_i} F\left(\frac{\theta}{T} \right) \right] = A^2 \tag{C15}$$

where

$$F\left(\frac{\theta}{T}\right) = \frac{\theta/T}{(e^{\theta/T}-1)} \left\{ \frac{1 + (\gamma_i-1) \frac{(\theta/T)e^{\theta/T}}{(e^{\theta/T}-1)} \left[1 + \frac{\theta/T}{(e^{\theta/T}-1)} \right]}{1 + \frac{(\gamma_i-1)}{\gamma_i} \frac{(\theta/T)^2 e^{\theta/T}}{(e^{\theta/T}-1)^2}} \right\} \tag{C16}$$

Now

$$\frac{\gamma T}{\gamma_i \theta} = \frac{a^2}{\gamma_i R \theta} \tag{C17}$$

For every value of T/θ there is thus a particular value of $a^2/\gamma_i R\theta$. The function $F(\theta/T)$ is therefore uniquely determined for any value of a^2 since $\gamma_i R\theta$ is of course a constant. With this point in mind, let

$$F(\theta/T) = G(a^2/\gamma_i R\theta) \tag{C18}$$

Figure 18 shows $G(a^2/\gamma_i R\theta)$ plotted as a function of $a^2/\gamma_i R\theta$. This curve is approximated with the following simple relation:

$$G(a^2/\gamma_i R\theta) = 0.38 \frac{a^2}{\gamma_i R\theta} + 0.71 - \frac{0.14}{a^2/\gamma_i R\theta} \tag{C19}$$

for $0.18 < \frac{a^2}{\gamma_i R\theta} < 1.0$

and

$$G(a^2/\gamma_i R\theta) = 0 \tag{C20}$$

for $0 < \frac{a^2}{\gamma_i R\theta} < 0.18$

Equation (C19) is also plotted in figure 18 to show the accuracy of this approximation. Consider first the case when G is given by equation (C19) which is written in the form

$$G(a^2/\gamma_i R\theta) = \xi a^2 + \mu + \eta \frac{1}{a^2} \tag{C21}$$

Where obviously

$$\left.\begin{aligned} \xi &= 0.38/\gamma_i R\theta \\ \mu &= 0.71 \\ \eta &= -0.14\ (\gamma_i R\theta) \end{aligned}\right\} \tag{C22}$$

Equation (C21) is substituted into equation (C15) and with equations (C18) and (C6) the following expression results:

$$\frac{2\xi}{\gamma_i}\Phi_\omega^4 + \left(\frac{\gamma_i+1}{\gamma_i-1} + \frac{2\mu}{\gamma_i}\right)\Phi_\omega^2 + \Phi^2 + \frac{2\eta}{\gamma_i} - A^2 = 0 \tag{C23}$$

In order to simplify this equation the following substitutions are made:

$$D^2 = \left(\frac{\gamma_i+1}{\gamma_i-1} + \frac{2\mu}{\gamma_i}\right)^2 + \frac{8}{\gamma_i}\xi\left(A^2 - \frac{2}{\gamma_i}\eta\right) \tag{C24}$$

$$\sin^2\nu = \frac{\frac{8\xi}{\gamma_i}\left(A^2 - \frac{2}{\gamma_i}\eta\right)}{D^2} \tag{C25}$$

$$\sin^2\tau = \frac{\frac{8\xi}{\gamma_i}\Phi^2}{D^2} \tag{C26}$$

and

$$\Phi_\omega^2 = \frac{D^2\cos^2\tau\,(\tau_\omega)^2}{\frac{8}{\gamma_i}\xi} \tag{C27}$$

Equation (C23) then reduces to

$$\cos^4 \tau \, (\tau_\omega)^4 + \frac{4 \cos \nu}{D} \cos^2 \tau \, (\tau_\omega)^2 + \frac{4 \sin^2 \tau}{D^2} - \frac{4 \sin^2 \nu}{D^2} = 0 \quad (C28)$$

This equation is solved for τ_ω, thus

$$\tau_\omega = \sqrt{\frac{2}{D}} \frac{1}{\cos \tau} \, (\cos \tau - \cos \nu)^{1/2} \quad (C29)$$

or

$$d\omega = \sqrt{\frac{D}{2}} \frac{\cos \tau \, d\tau}{(\cos \tau - \cos \nu)^{1/2}} \quad (C30)$$

This expression is readily integrated to obtain the following equation relating ω to the local velocity:

$$\omega - \omega_N = \sqrt{D} \left\{ 2 \left[E(k,z) - E(k,z_N) \right] - \left[F(k,z) - F(k, z_N) \right] \right\} \quad (C31)$$

where

E elliptic integral of the second kind

F elliptic integral of the first kind

k $\sin \frac{\nu}{2}$ (modulus)

z $\sin^{-1} \left(\frac{\sin \tau/2}{\sin \nu/2} \right)$ (amplitude)

The procedure for calculating corresponding values of the pressure, p, and the deflection angle, δ, is straightforward with the aid of the preceding equations and may be summarized as follows:

1. Calculate A^2, equation (C9)
2. Calculate D^2, equation (C24)
3. Calculate ν, equation (C25)
4. Assume a value of T, less than T_N
5. Calculate p, equations (16) and (17)
6. Calculate V^2, equation (C8)
7. Calculate γ, equation (C14)

8. Calculate a^2 (or Φ_ω^2), equation (C11)
9. Calculate M and, in turn, β from V and a
10. Calculate u^2 (or Φ^2), equation (C7)
11. Calculate τ, equation (C26)
12. Calculate ω, equation (C31)
13. Calculate δ, equation (C1)

This procedure is followed so long as the quantity $a^2/\gamma_1 R\theta$ is greater than 0.18. (This is equivalent to the temperature being greater than approximately 1000° R.) For values of $a^2/\gamma_1 R\theta$ less than or equal to 0.18 (or temperatures less than about 1000° R) G is set equal to zero (see equation (C20)). In this case equation (C15) reduces to the same form as for an ideal gas, and therefore the well-known ideal gas relationships can be used.

APPENDIX D

EVALUATION OF THE DISTURBANCE STRENGTH RATIO

Consider the element of an oblique shock wave shown in the accompanying sketch

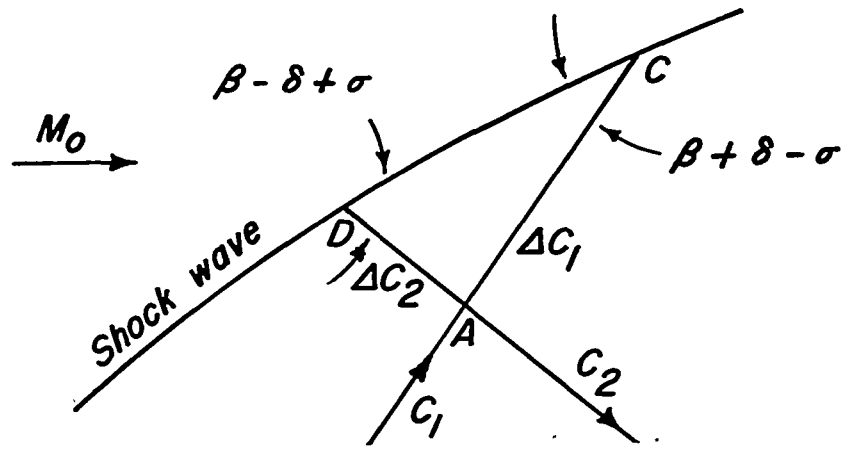

It is evident that the ratio $\dfrac{\partial\delta/\partial C_1}{\partial\delta/\partial C_2}$ is a measure of the ratio of strengths of reflected and incident disturbances, respectively, since all disturbances incident on the wave between points D and C must travel along first-family characteristics which cross C_2 between D and A, while all disturbances reflected from the shock wave in this region must travel along second-family characteristics which cross C_1 between A and C. This ratio, termed the disturbance strength ratio, may be evaluated locally just downstream of the shock wave in the following manner. The points D and C are chosen sufficiently close together so that the difference in pressure between these points may be written

$$p_C - p_D = \frac{\partial p}{\partial C_2}\Delta C_2 + \frac{\partial p}{\partial C_1}\Delta C_1 \qquad (D1)$$

or

$$p_C - p_D = \left.\frac{dp}{d\delta}\right|_N (\delta_C - \delta_D) \qquad (D2)$$

where $\left.\frac{dp}{d\delta}\right|_N$ is the rate of change of pressure with flow deflection angle on the downstream side of the wave. Now the change in deflection angle between D and C is given by the relation

$$\delta_C-\delta_D = \frac{\partial\delta}{\partial C_2}\Delta C_2 + \frac{\partial\delta}{\partial C_1}\Delta C_1 \tag{D3}$$

Thus equations (D2) and (D3) combine to yield

$$p_C-p_D = \left.\frac{dp}{d\delta}\right|_N\left(\frac{\partial\delta}{\partial C_2}\Delta C_2+\frac{\partial\delta}{\partial C_1}\Delta C_1\right) \tag{D4}$$

But the compatibility equations (equations (12) and (13)) combine with equation (D1) to give

$$p_C-p_D = \frac{2\gamma_N p_N}{\sin 2\beta_N}\left(\frac{\partial\delta}{\partial C_2}\Delta C_2 - \frac{\partial\delta}{\partial C_1}\Delta C_1\right) \tag{D5}$$

Equating the right-hand members of this and the previous expression and rearranging, there is then obtained

$$\frac{\partial\delta/\partial C_1}{\partial\delta/\partial C_2} = \frac{\left(\frac{2\gamma_N p_N}{\sin 2\beta_N} - \left.\frac{dp}{d\delta}\right|_N\right)}{\left(\frac{2\gamma_N p_N}{\sin 2\beta_N}+\left.\frac{dp}{d\delta}\right|_N\right)}\left(\frac{\Delta C_2}{\Delta C_1}\right) \tag{D6}$$

The ratio $\frac{\Delta C_2}{\Delta C_1}$ follows from the sine law, however; thus the disturbance strength ratio is given by the relation

$$\frac{\partial\delta/\partial C_1}{\partial\delta/\partial C_2} = \frac{\left(\frac{2\gamma_N p_N}{\sin 2\beta_N} - \left.\frac{dp}{d\delta}\right|_N\right)}{\left(\frac{2\gamma_N p_N}{\sin 2\beta_N} + \left.\frac{dp}{d\delta}\right|_N\right)}\frac{\sin(\beta_N+\delta_N-\sigma)}{\sin(\beta_N-\delta_N+\sigma)} \tag{D7}$$

which holds for both ideal and calorically imperfect gas flows.

If the shock wave is attached to the airfoil at the leading edge (or more properly if $M_N \geq 1$), this expression may be used with equation (23) to determine the surface pressure gradient at that point. A calculation analogous to this for ideal gas flows has already been carried out by Crocco, Schaefer, Munk and Prim and others as discussed previously.

REFERENCES

1. Ackeret, J.: Air Forces on Airfoils Moving Faster than Sound. NACA TM 317, 1925.

2. Busemann, A., and Walchner, O.: Airfoil Characteristics at Supersonic Speeds. British R.T.P. Trans. 1786. (Forschung auf dem gebeite des Ingenieurwesens, vol. 4, no. 2, March/April 1933, pp. 87-92.)

3. Epstein, Paul S.: On the Air Resistance of Projectiles. Proceedings of the National Academy of Sciences, vol. 17, 1931, pp. 532-547.

4. Eggers, A. J., Jr.: One-Dimensional Flows of an Imperfect Diatomic Gas. NACA Rep. 959, 1950. (Formerly NACA TN 1861)

5. Ivey, H. Reese, and Cline, Charles W.: Effect of Heat-Capacity Lag on the Flow Through Oblique Shock Waves. NACA TN 2196, 1950.

6. Bethe, H. A., and Teller, E.: Deviations from Thermal Equilibrium in Shock Waves. Ballistic Research Lab. Rept. No. X-117. Aberdeen Proving Ground, Aberdeen, Maryland, 1945.

7. Crocco, Luigi: Singolarita della Corrente Gassosa Iperacustica Nell'Intorno di una Prora a Diedro. L'Aerotecnica, vol. 17, no. 6, June 1937, pp. 519-534.

8. Schaefer, M.: The Relation Between Wall Curvature and Shock Front Curvature in Two-Dimensional Gas Flow. USAF Tech. Rept. F-TS-1202-IA, Jan. 1949.

9. Munk, M. M., and Prim, R. C.: Surface-Pressure Gradient and Shock-Front Curvature at the Edge of a Plane Ogive with Attached Shock Front. Jour. Aero. Sci., vol. 15, no. 11, Nov. 1948, pp. 691-695.

10. Chapman, Dean R.: Airfoil Profiles for Minimum Pressure Drag at Supersonic Velocities - General Analysis With Application to Linearized Supersonic Flow. NACA TN 2264, 1951.

11. Isenberg, J. S.: The Method of Characteristics in Compressible Flow. Part I (Steady Supersonic Flow) USAF Tech. Rept. F-TR-1173A-ND, Air Materiel Command, Wright Field, Technical Intelligence (Brown University, Graduate Division of Applied Mathematics, A-9-M 11/1), Dec. 1947.

12. Thomas, T. Y.: The Determination of Pressure on Curved Bodies behind Shocks. Communications on Pure and Applied Mathematics, vol. III, no. 2, June 1950, pp. 103-132.

13. Noyes, Robert N.: Prandtl-Meyer Flow for a Diatomic Gas of Variable Specific Heat. NACA TN 2125, 1950.

14. Tsien, Hsue-shen: Similarity Laws of Hypersonic Flows, Jour. Math. and Phys., vol. 25, no. 3, Oct. 1946, pp. 247-251.

15. Linnell, Richard D.: Two-Dimensional Airfoils in Hypersonic Flows. Jour. Aero. Sci., vol. 16, no. 1, Jan. 1949, pp. 22-30.

16. Lighthill, M. J.: The Flow Behind a Stationary Shock. Philosophical Magazine, ser. 7, vol. 40, Feb. 1949, pp. 214-220.

17. Rand, Robert C.: Prandtl-Meyer Flow Behind a Curved Shock Wave. Jour. Math. and Phys., vol. 29, no. 2, July 1950, pp. 124-132.

18. Busemann, A.: Flussigkeits-und Garbewegung. Handwörterbuch der Naturwissenschaften, Zweite Auflage, Gustav Fischer, Jena, 1933, pp. 266-279.

19. Ivey, H. Reese, Klunker, E. Bernard, and Bowen, Edward N.: A Method for Determining the Aerodynamic Characteristics of Two- and Three-Dimensional Shapes at Hypersonic Speeds. NACA TN 1613, 1948.

20. Meyer, Th.: The Two-Dimensional Phenomena of Motion in a Gas Flowing at Supersonic Velocity. Cornell Research Foundation, Inc., Buffalo, New York, Aug. 1945. (Translation from: Mitteilungen über Forschungsarbeiten auf dem Gebiete des Ingenieurwesens, Heft 62, 1908, pp. 31-67.)

TABLE I.- TABLE OF FUNCTIONS FOR SLENDER-AIRFOIL METHOD

$M_o\delta_N$	$\gamma = \gamma_i$		$\gamma = \gamma_a$ ($T_o = 500^oR$)		
	$g(M_o\delta_N)$	$f(M_o\delta_N)$	γ_a	$g(M_o\delta_N)$	$f(M_o\delta_N)$
0	1.000	0	1.400	1.000	0
.05	1.072	.009901	1.400	1.072	.009897
.10	1.148	.01961	1.400	1.149	.01959
.15	1.230	.02912	1.400	1.230	.02909
.20	1.316	.03845	1.400	1.316	.03841
.25	1.406	.04760	1.400	1.406	.04755
.30	1.502	.05656	1.399	1.502	.05649
.35	1.604	.06537	1.399	1.603	.06524
.40	1.710	.07393	1.399	1.710	.07380
.45	1.823	.08235	1.399	1.822	.08220
.50	1.941	.09058	1.399	1.940	.09040
.55	2.065	.09863	1.399	2.064	.09841
.60	2.195	.1071	1.399	2.194	.1062
.65	2.332	.1142	1.399	2.330	.1139
.70	2.474	.1217	1.399	2.473	.1213
.75	2.624	.1290	1.398	2.622	.1286
.80	2.780	.1362	1.398	2.777	.1356
.85	2.943	.1431	1.398	2.939	.1425
.90	3.112	.1499	1.398	3.108	.1492
.95	3.289	.1565	1.398	3.284	.1557
1.00	3.473	.1630	1.397	3.466	.1620
1.1	3.862	.1753	1.396	3.852	.1740
1.2	4.280	.1869	1.396	4.266	.1853
1.3	4.728	.1978	1.395	4.708	.1958
1.4	5.206	.2064	1.393	5.179	.2056
1.5	5.715	.2178	1.392	5.679	.2147
1.6	6.256	.2269	1.391	6.207	.2232
1.7	6.827	.2354	1.389	6.764	.2309
1.8	7.431	.2433	1.388	7.349	.2381
1.9	8.066	.2507	1.386	7.962	.2447
2.0	8.734	.2577	1.384	8.605	.2508
2.1	9.411	.2646	1.382	9.274	.2564
2.2	10.17	.2702	1.380	9.973	.2616
2.3	10.93	.2759	1.378	10.70	.2664
2.4	11.73	.2812	1.376	11.46	.2709
2.5	12.56	.2862	1.374	12.24	.2749
2.6	13.42	.2908	1.372	13.06	.2788
2.7	14.32	.2951	1.370	13.90	.2823
2.8	15.25	.2992	1.369	14.77	.2856
2.9	16.21	.3030	1.367	15.68	.2887

TABLE I.- CONTINUED

$M_o\delta_N$	$\gamma = \gamma_i$		$\gamma = \gamma_a$ ($T_o = 500^oR$)		
	$g(M_o\delta_N)$	$f(M_o\delta_N)$	γ_a	$g(M_o\delta_N)$	$f(M_o\delta_N)$
3.0	17.21	0.3066	1.365	16.61	0.2916
3.2	19.30	.3130	1.362	18.56	.2968
3.4	21.52	.3187	1.360	20.64	.3015
3.6	23.88	.3237	1.358	22.83	.3057
3.8	26.38	.3280	1.356	25.16	.3094
4.0	29.00	.3322	1.354	27.60	.3128
4.2	31.76	.3358	1.352	30.17	.3158
4.4	34.65	.3389	1.351	32.86	.3186
4.6	37.68	.3418	1.350	35.68	.3211
4.8	40.84	.3443	1.349	38.63	.3234
5.0	44.14	.3466	1.349	41.70	.3255
5.2	47.56	.3487	1.348	44.91	.3275
5.4	51.13	.3506	1.347	48.23	.3292
5.6	54.82	.3523	1.347	51.68	.3309
5.8	58.66	.3539	1.346	55.26	.3323
6.0	62.62	.3553	1.346	58.96	.3337
6.2	66.73	.3566	1.346	62.79	.3350
6.4	70.96	.3578	1.345	66.77	.3363
6.6	75.33	.3589			
6.8	79.83	.3600			
7.0	84.47	.3610			
7.2	89.24	.3618			
7.4	94.15	.3626			
7.6	99.19	.3633			
7.8	104.4	.3640			
8.0	109.7	.3647			
8.5	123.5	.3661			
9.0	138.2	.3673			
9.5	153.8	.3684			
10.0	170.2	.3693			
10.5	187.4	.3701			
11.0	205.4	.3707			
11.5	224.3	.3714			
12.0	244.1	.3719			
12.5	264.7	.3723			
13.0	286.1	.3727			
13.5	308.3	.3731			
14.0	331.4	.3735			
14.5	355.4	.3738			
15.0	380.2	.3740			

TABLE I.- CONCLUDED

$M_o\delta_N$	$\gamma = \gamma_i$		$\gamma = \gamma_a$ ($T_o = 500^oR$)		
	$g(M_o\delta_N)$	$f(M_o\delta_N)$	γ_a	$g(M_o\delta_N)$	$f(M_o\delta_N)$
16.0	432.3	0.3745			
17.0	487.7	.3749			
18.0	546.5	.3752			
19.0	608.6	.3755			
20.0	674.2	.3757			
22.0	815.3	.3761			
24.0	969.8	.3764			
26.0	1138	.3766			
28.0	1319	.3768			
30.0	1514	.3770			
35.0	2060	.3772			
40.0	2690	.3774			
45.0	3404	.3775			
50.0	4202	.3776			
60.0	6050	.3777			
70.0	8233	.3778			
80.0	10750	.3778			
90.0	13610	.3779			
100.0	16800	.3779			
∞	∞	.3780			

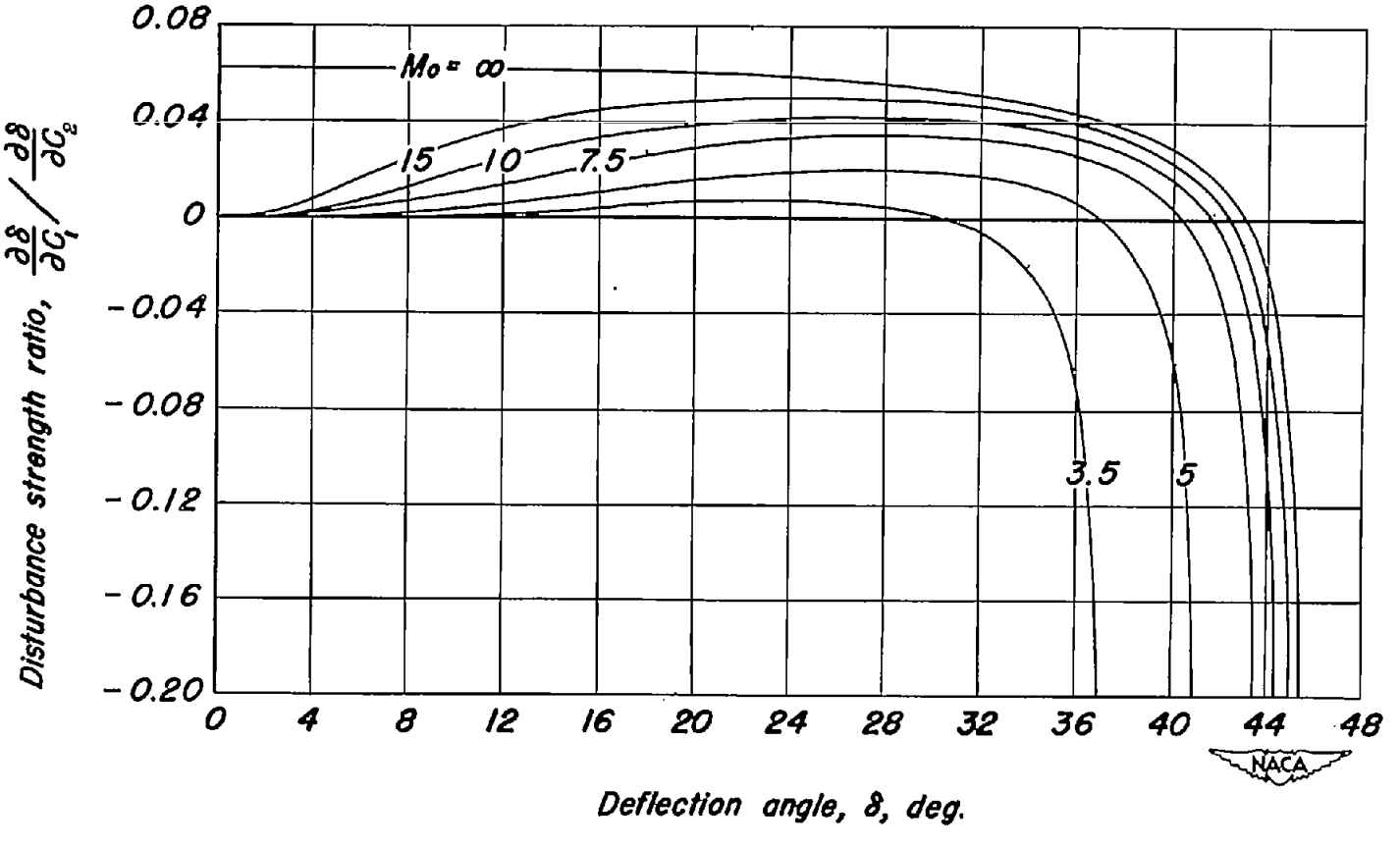

Figure 1.— Variation with deflection angle of the disturbance strength ratio behind an oblique shock wave for various free-stream Mach numbers ($\gamma = 1.4$).

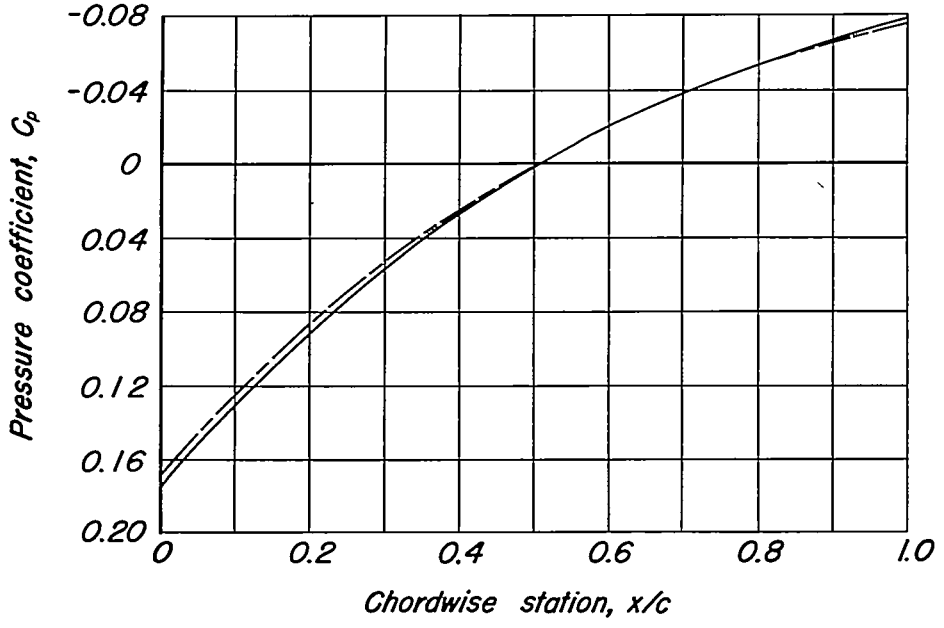

(a) $M_o = 3.5$

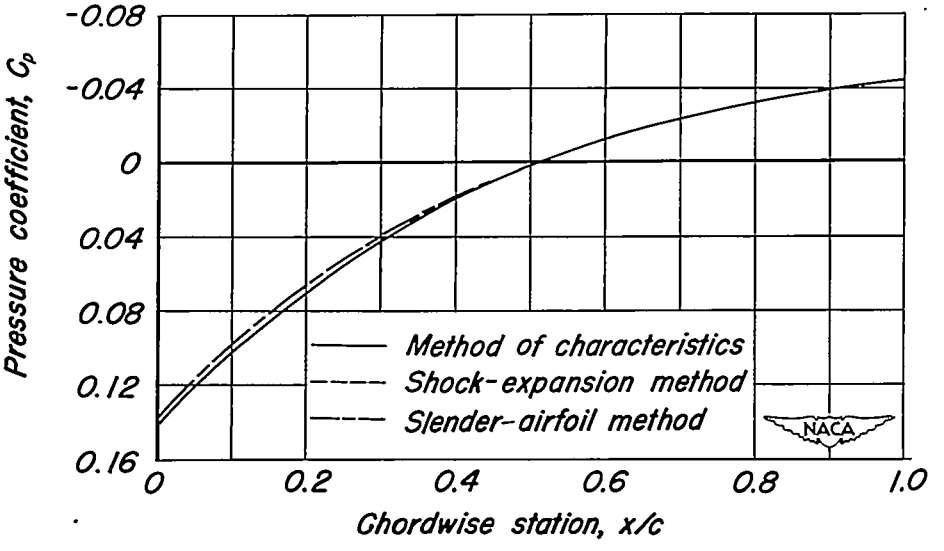

(b) $M_o = 5$

Figure 2. — Pressure distribution on 10-percent-thick biconvex airfoil section for various free-stream Mach numbers at $\alpha = 0°$

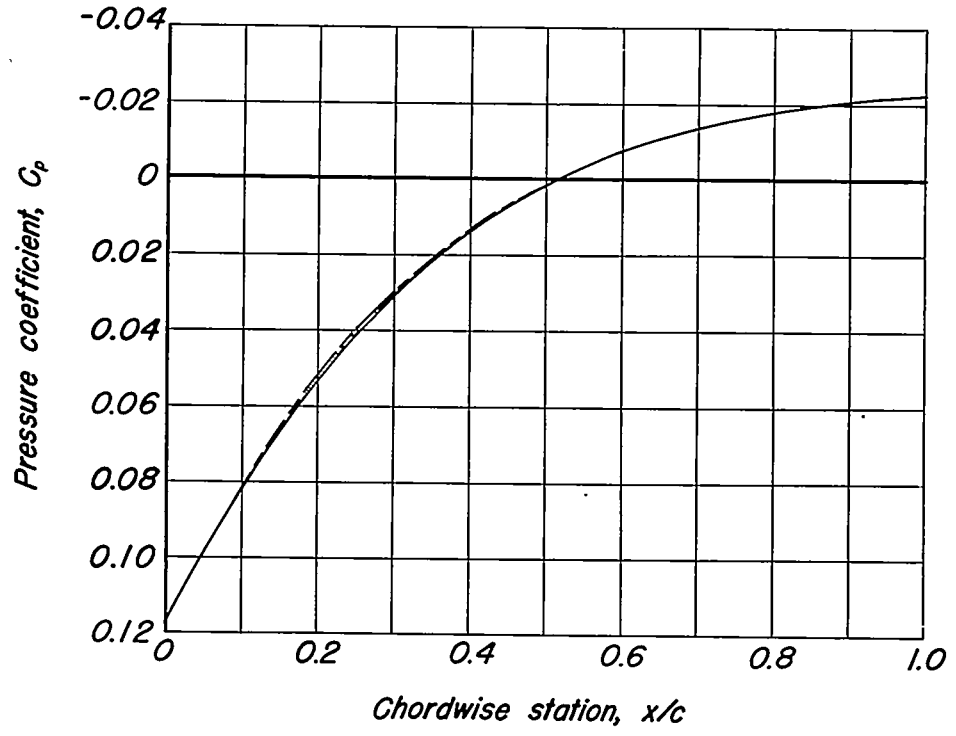

(c) $M_o = 7.5$

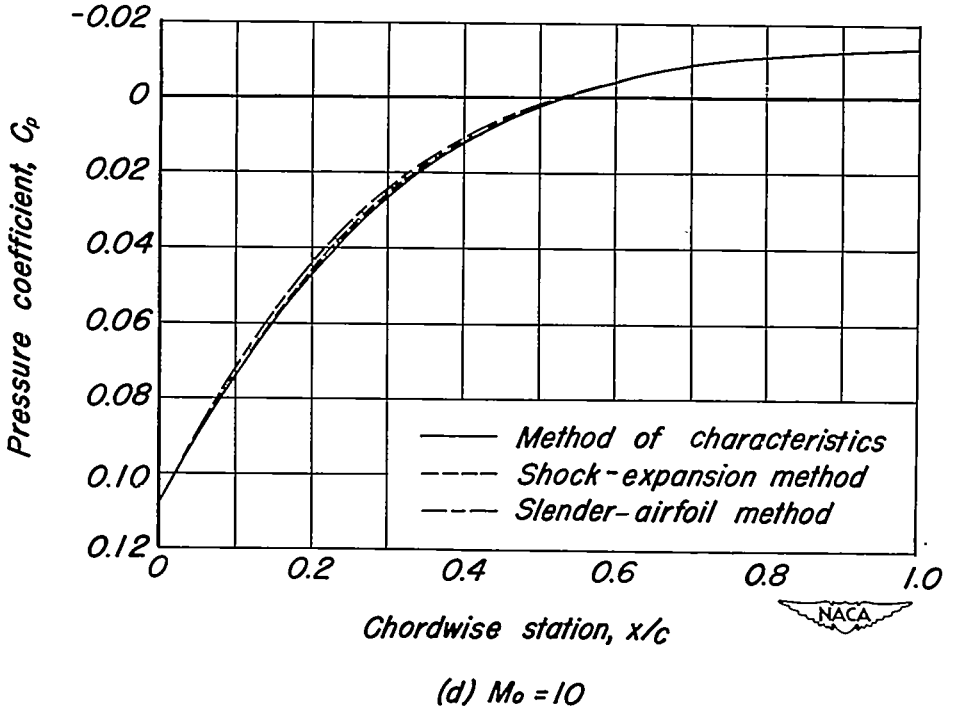

(d) $M_o = 10$

Figure 2. – continued.

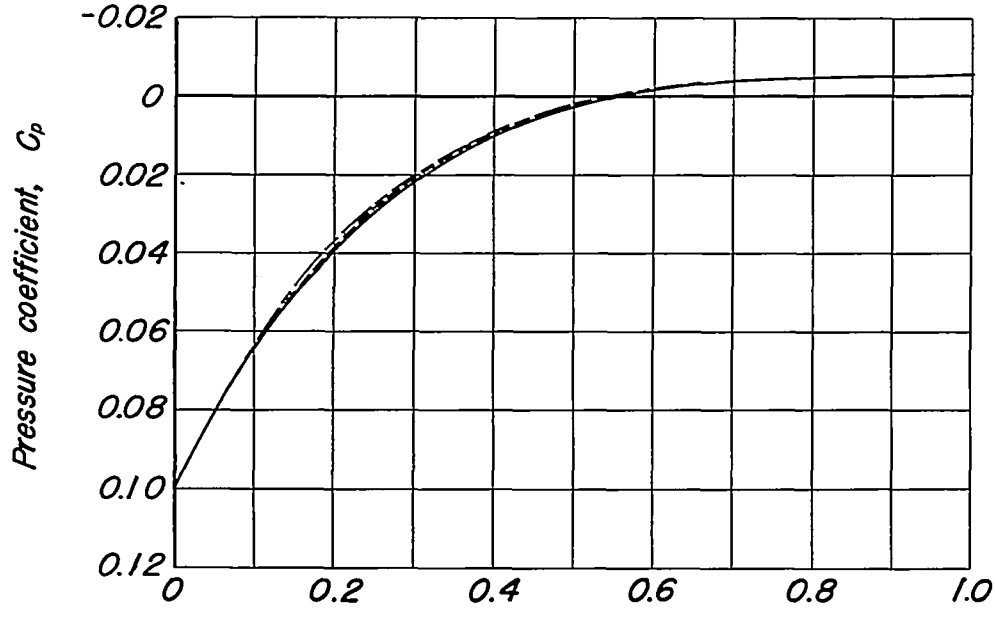

(e) $M_o = 1.5$

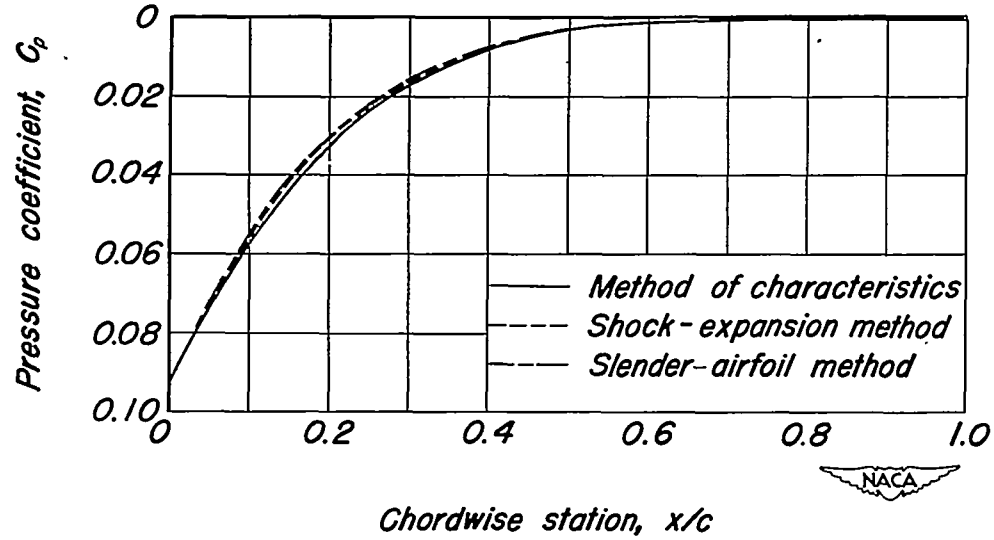

(f) $M_o = \infty$

Figure 2. – concluded.

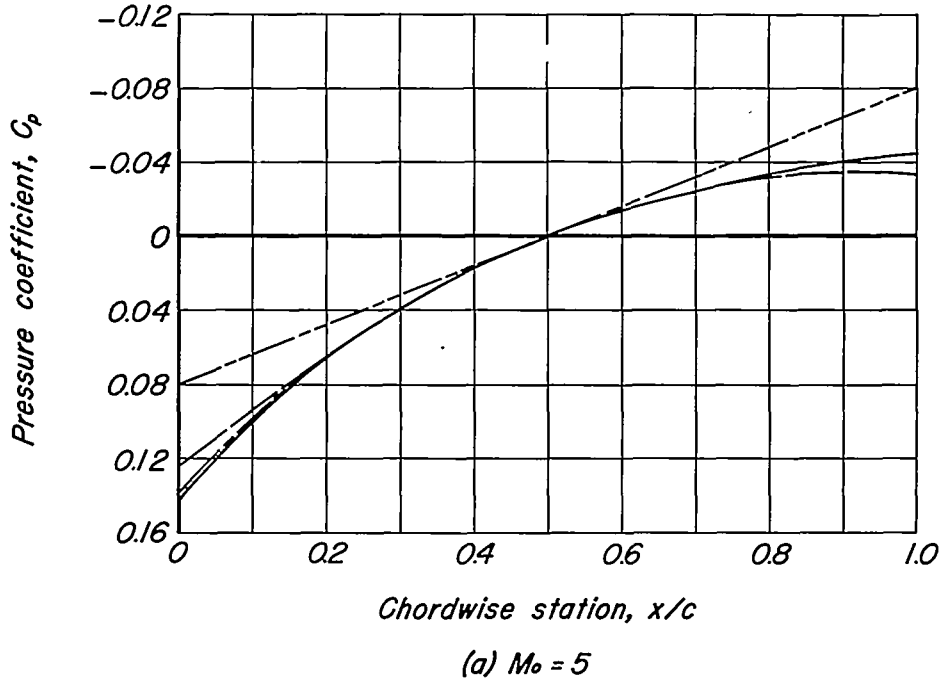

(a) $M_o = 5$

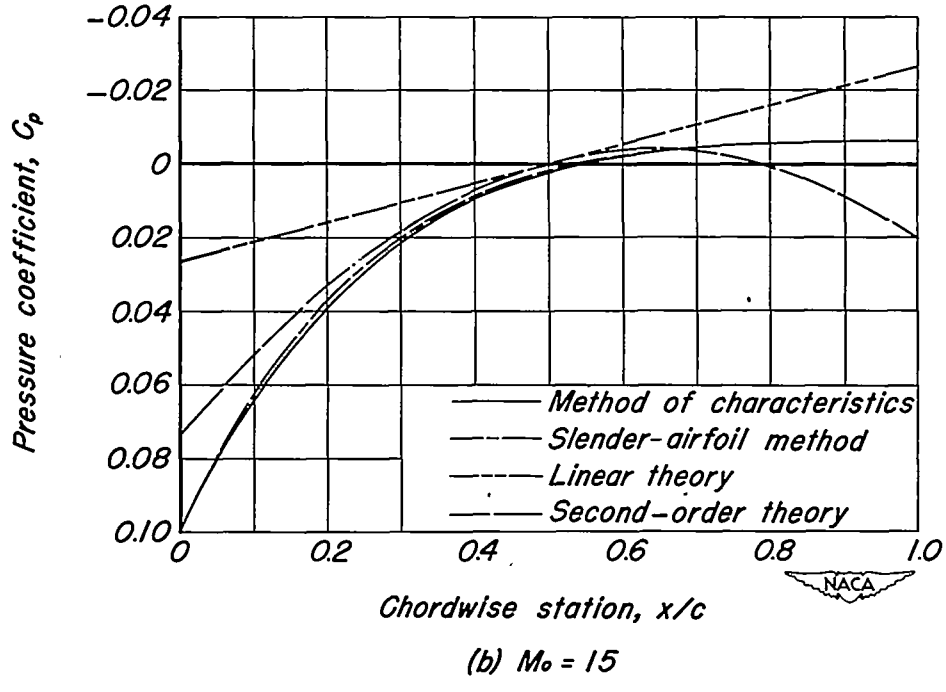

(b) $M_o = 15$

Figure 3.- Pressure distribution on 10-percent-thick biconvex airfoil section at $\alpha = 0°$

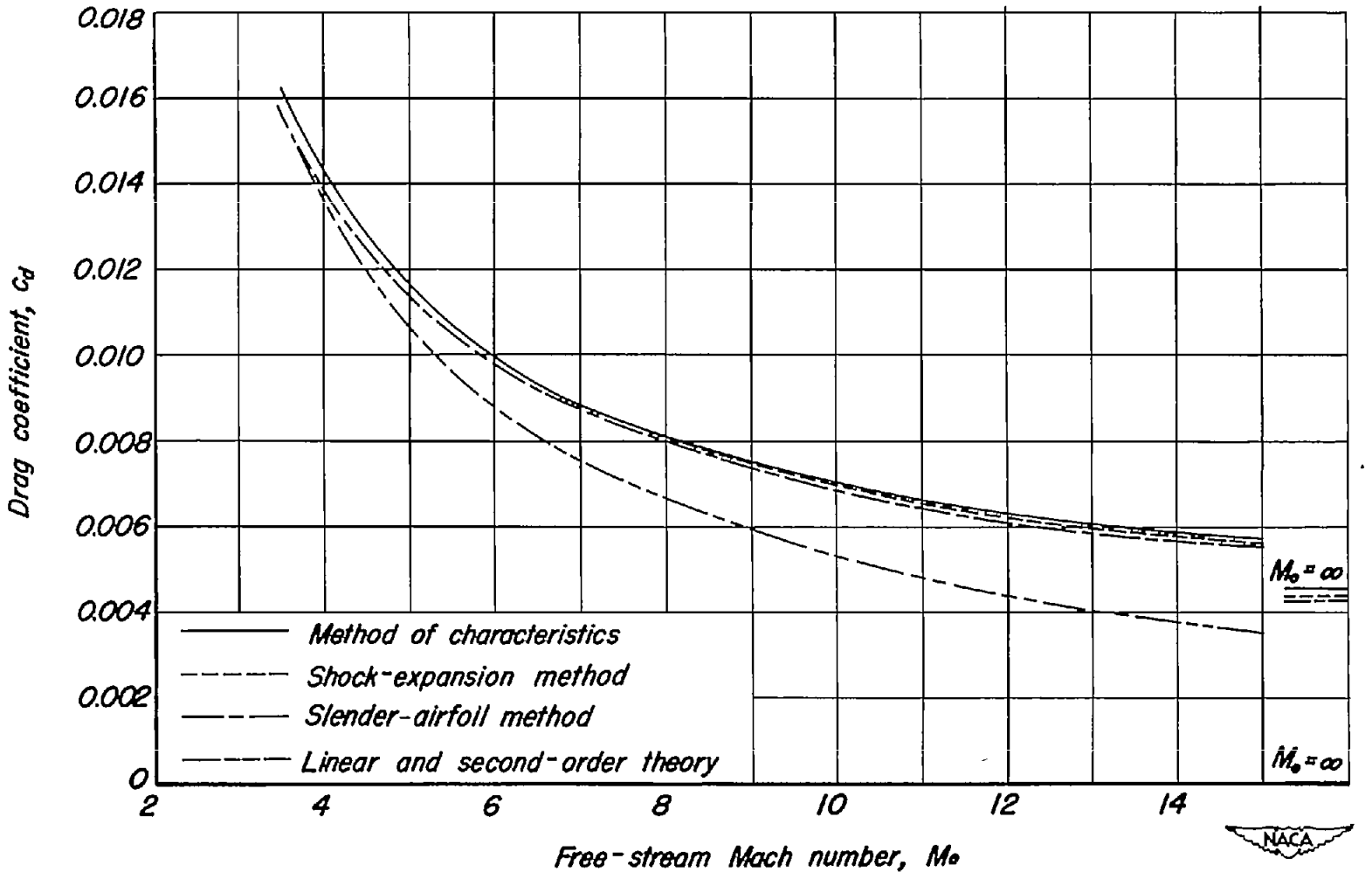

Figure 4. — Variation of drag coefficient with free-stream Mach number for 10-percent-thick biconvex airfoil section at $\alpha = 0°$ ($\gamma = 1.4$).

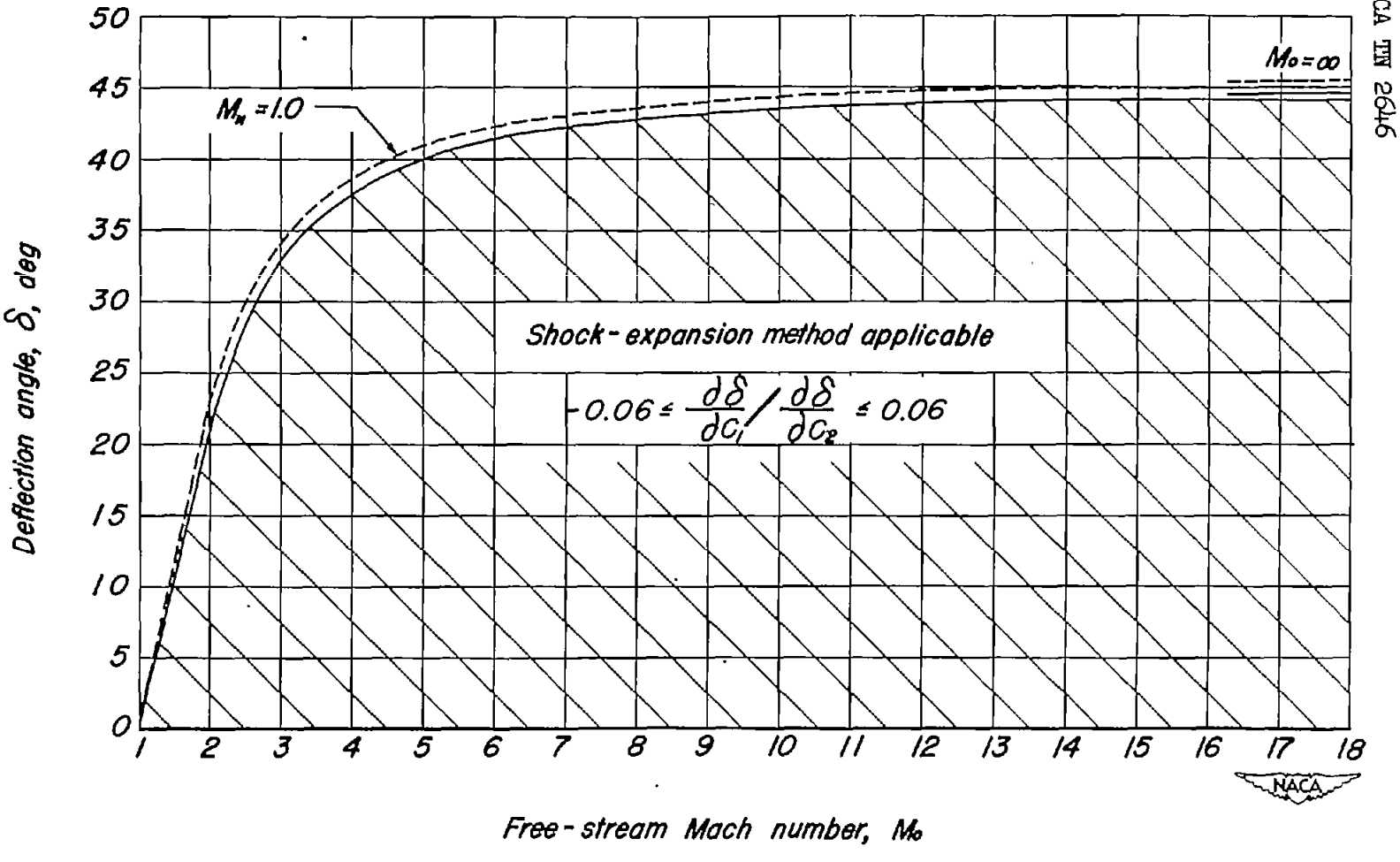

Figure 5.– Range of applicability of shock-expansion method ($\gamma = 1.4$).

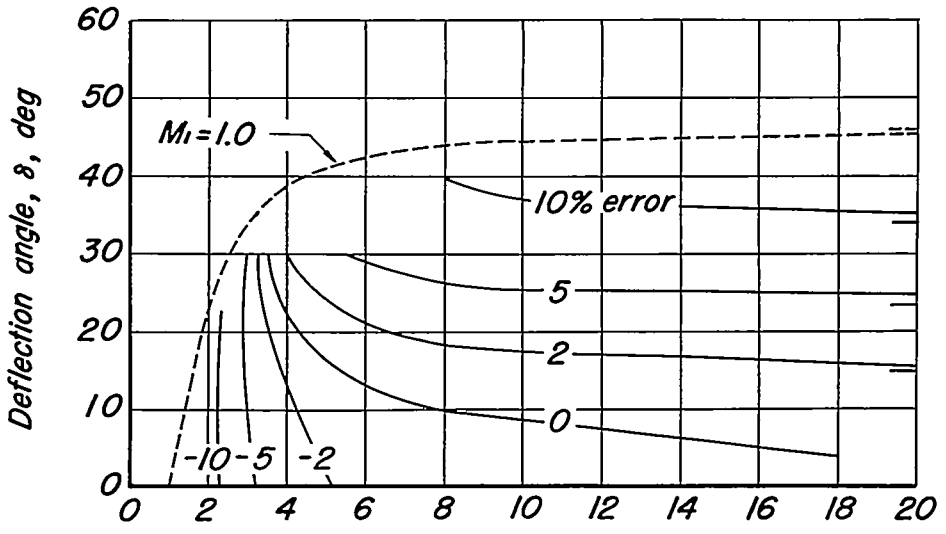

Free-stream Mach number, M_∞

(a) Oblique shock-wave flows

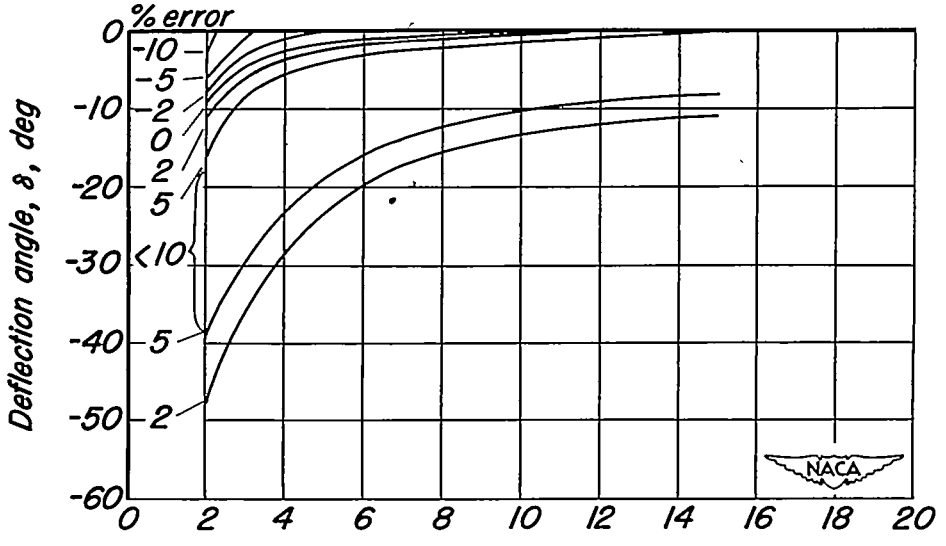

Free-stream Mach number, M_∞

(b) Expansion flows

Figure 6.—Accuracy of slender-airfoil method in predicting pressure coefficients (γ=1.4).

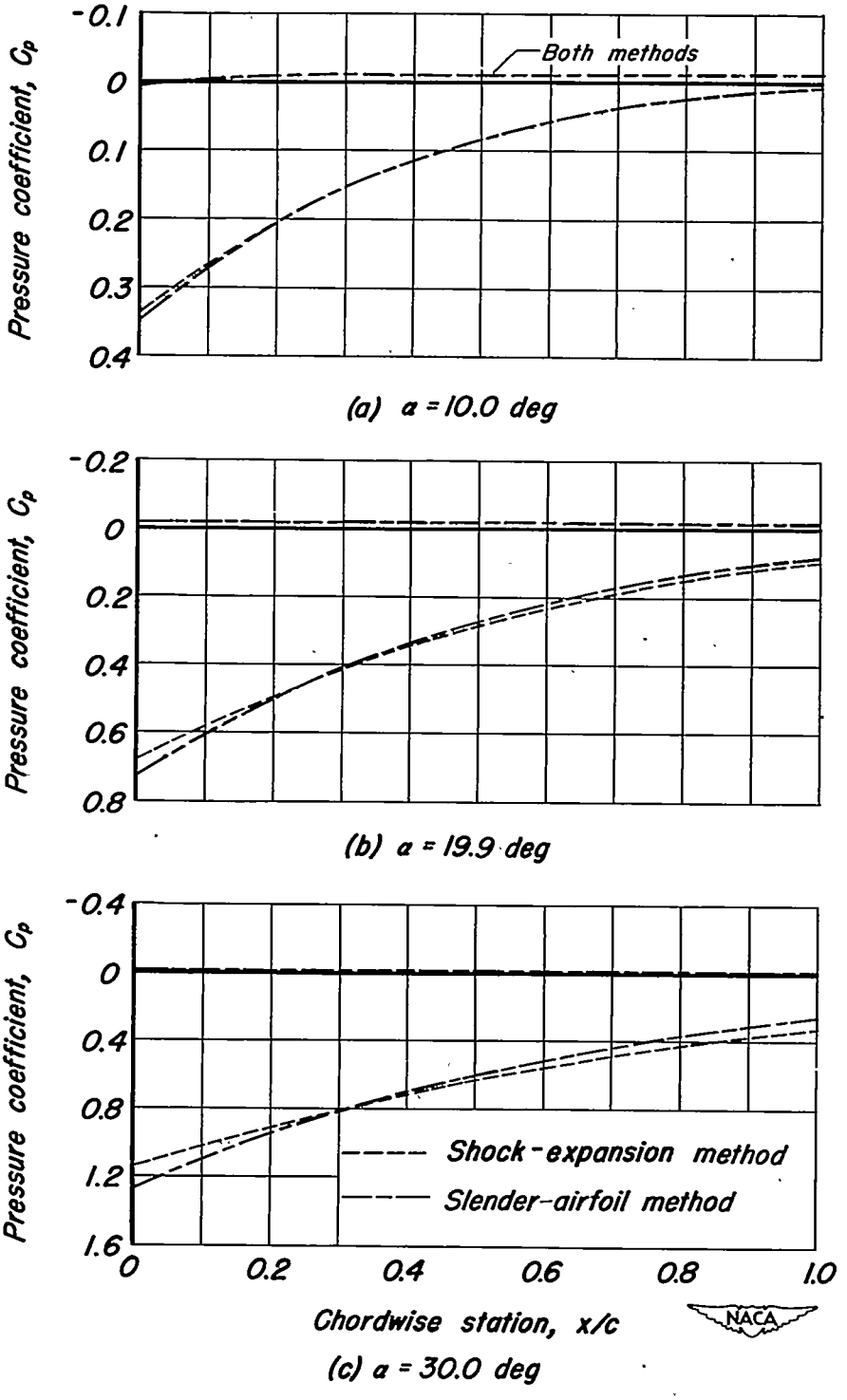

Figure 7. — Pressure distribution on 10-percent-thick biconvex airfoil section for various angles of attack at M_0 = 10 (γ = 1.4).

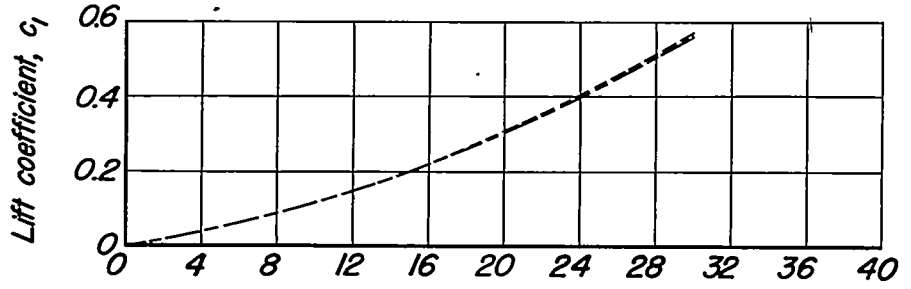

(a) Lift coefficient.

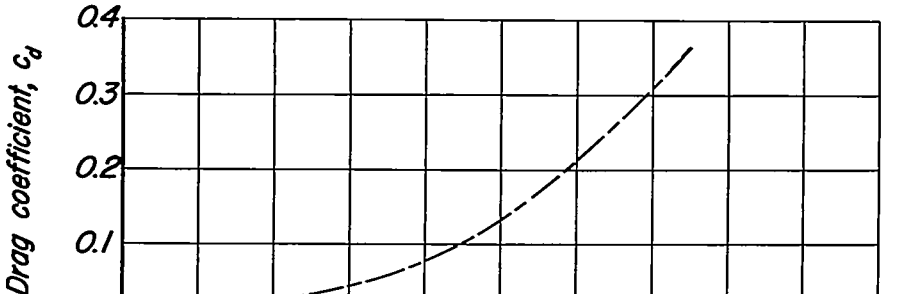

(b) Drag coefficient.

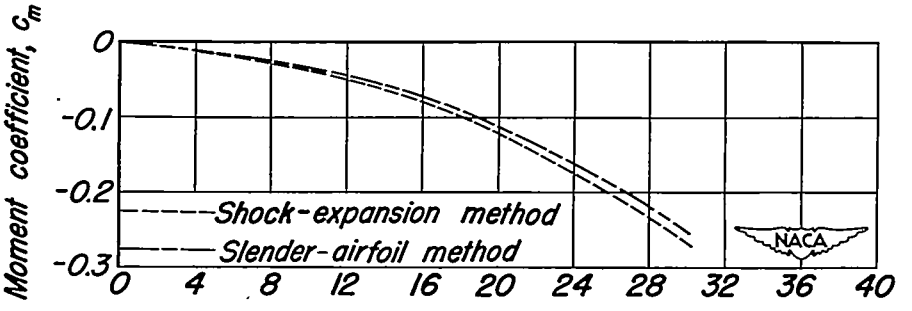

(c) Moment coefficient.

Figure 8.— Variation of force and moment coefficients with angle of attack for 10-percent-thick biconvex airfoil section at $M_\infty = 10$ ($\gamma = 1.4$).

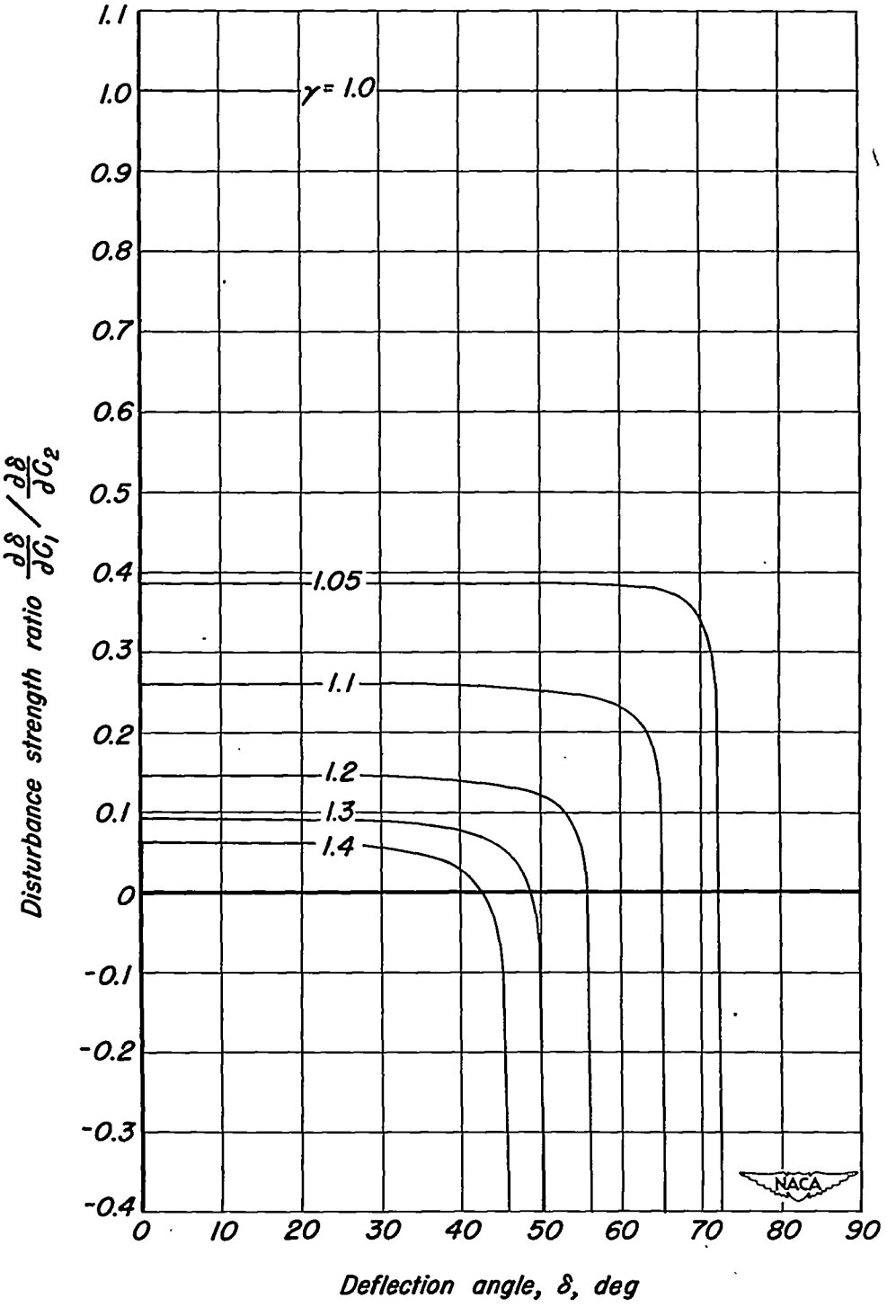

Figure 9. – Variation of disturbance strength ratio with deflection angle at infinite free-stream Mach number for various values of γ.

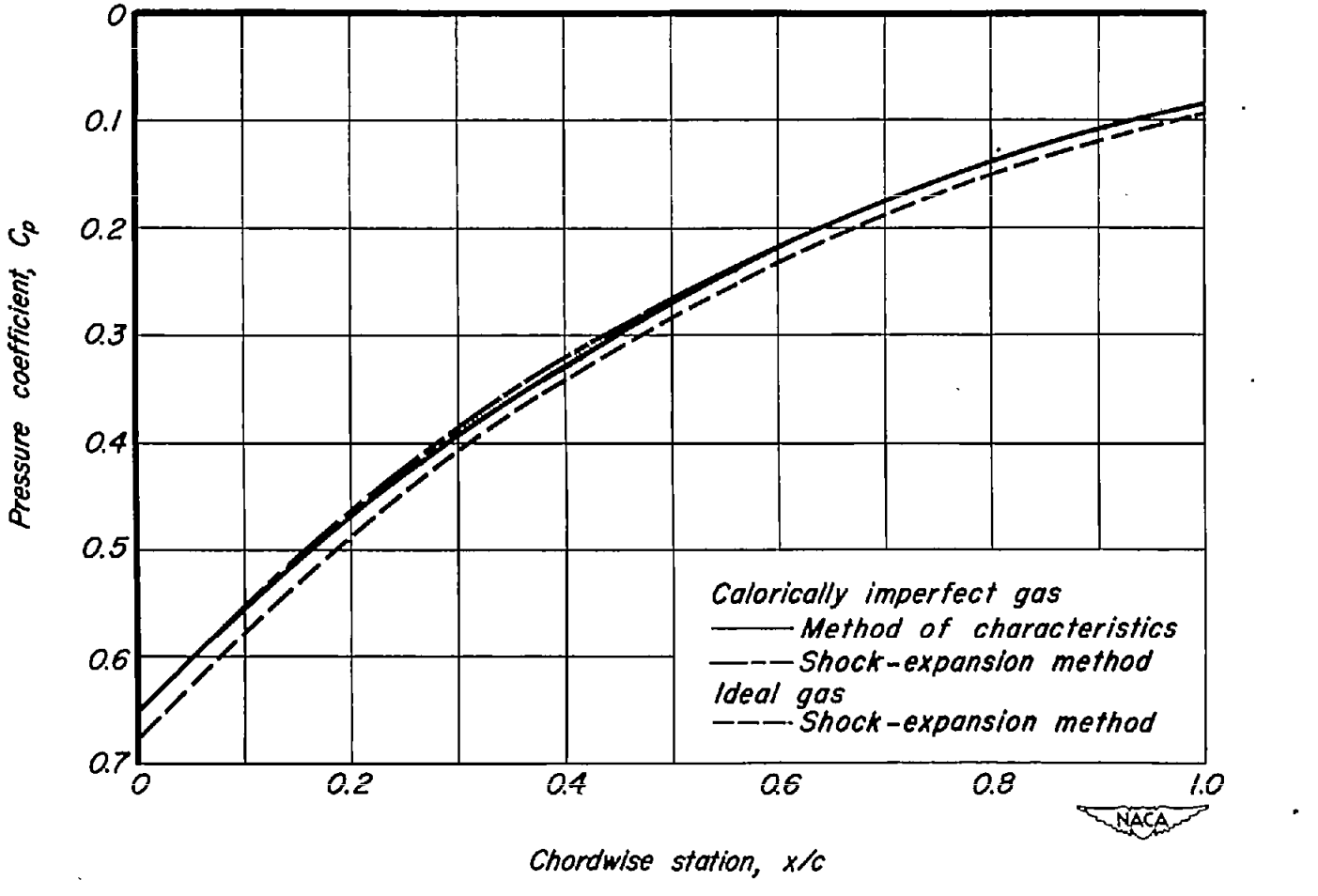

Figure 10.– Pressure distribution on lower surface of 10-percent-thick biconvex airfoil section at $M_0 = 10$, $T_0 = 500°$ R, $\alpha = 19.9°$

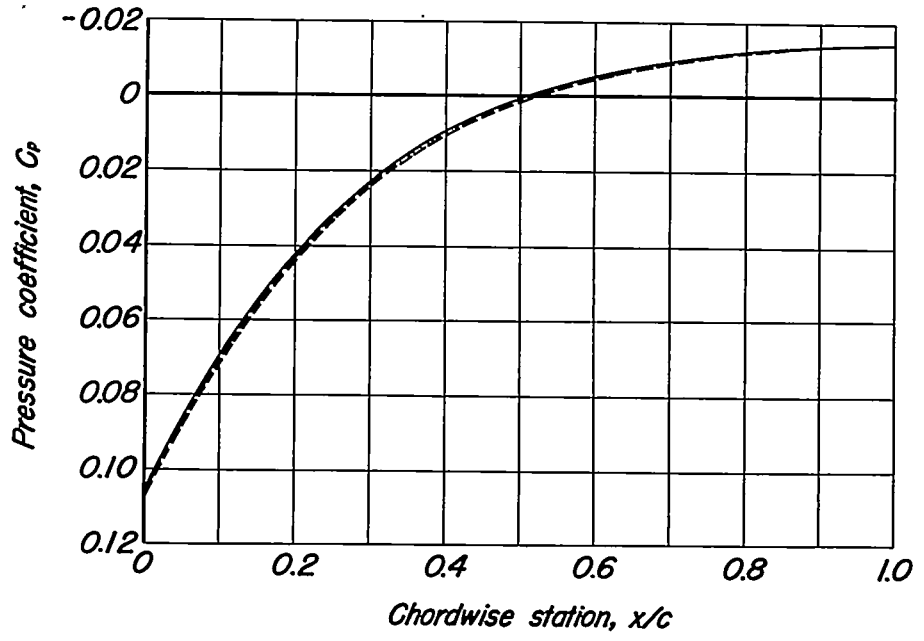

(a) $\alpha = 0°$

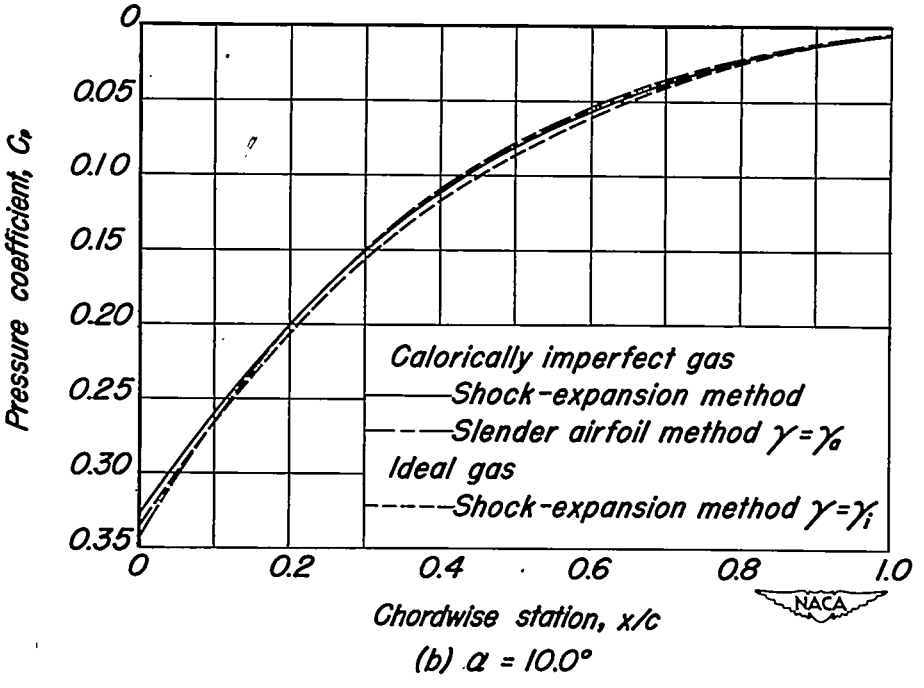

(b) $\alpha = 10.0°$

Figure 11.— Pressure distribution on lower surface of 10-percent-thick biconvex airfoil section for various angles of attack at $M_\infty = 10$ and $T_\infty = 500°$ R.

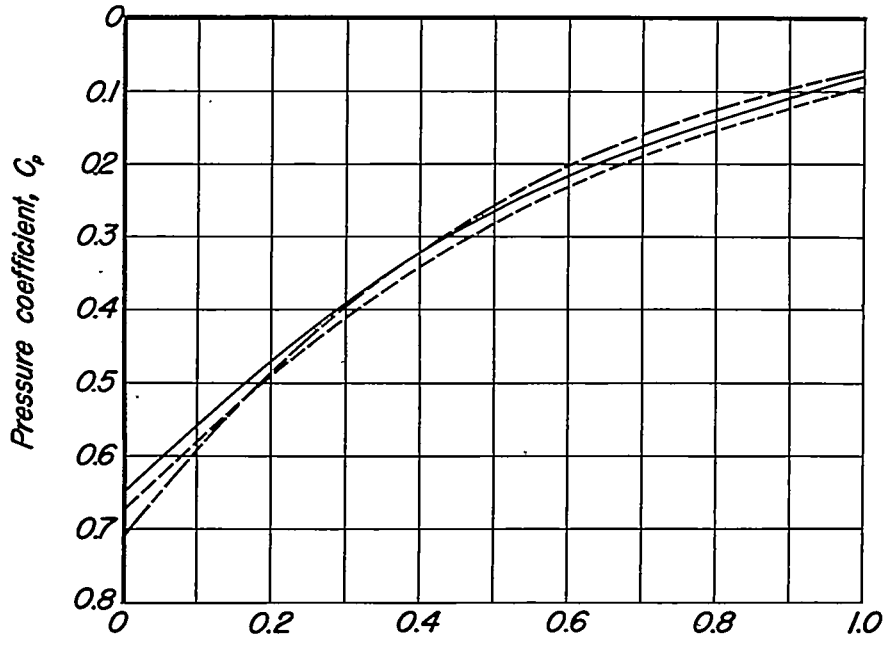

(c) $\alpha = 19.9°$

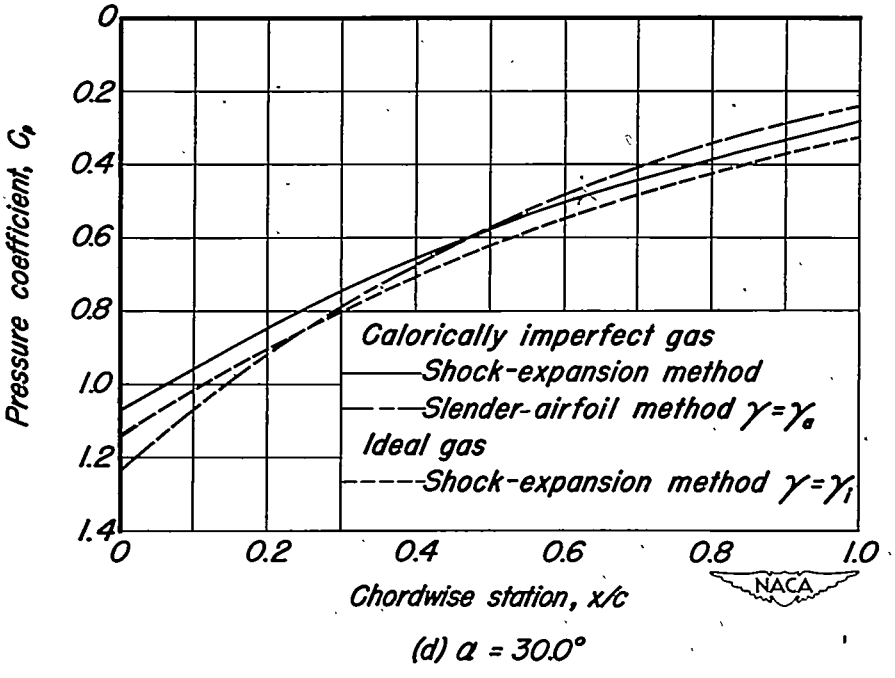

(d) $\alpha = 30.0°$

Figure 11. – Concluded.

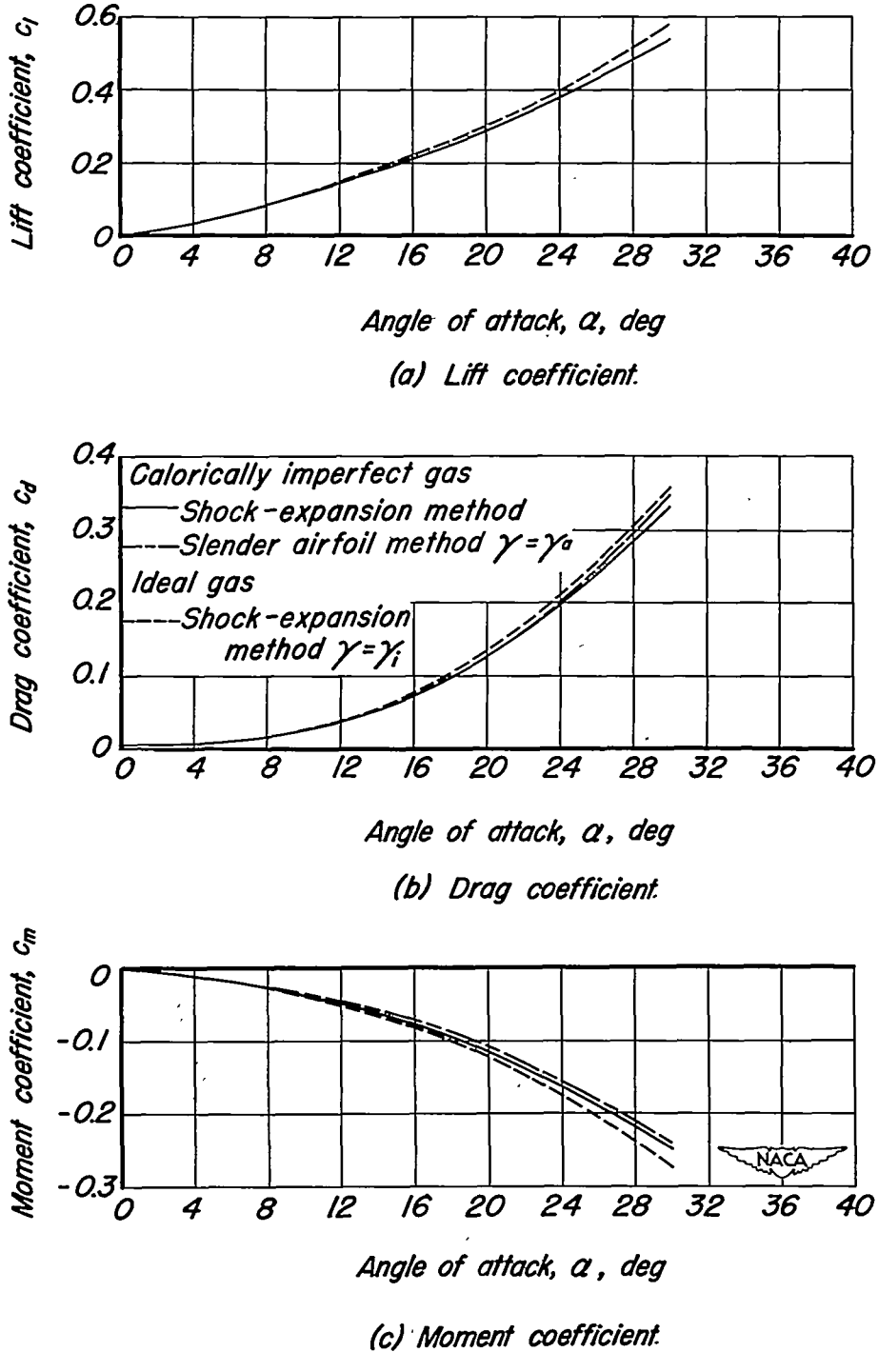

Figure 12.– Variation of force and moment coefficients with angle of attack for 10-percent-thick biconvex airfoil section at $M_\infty = 10$, $T_\infty = 500°R$.

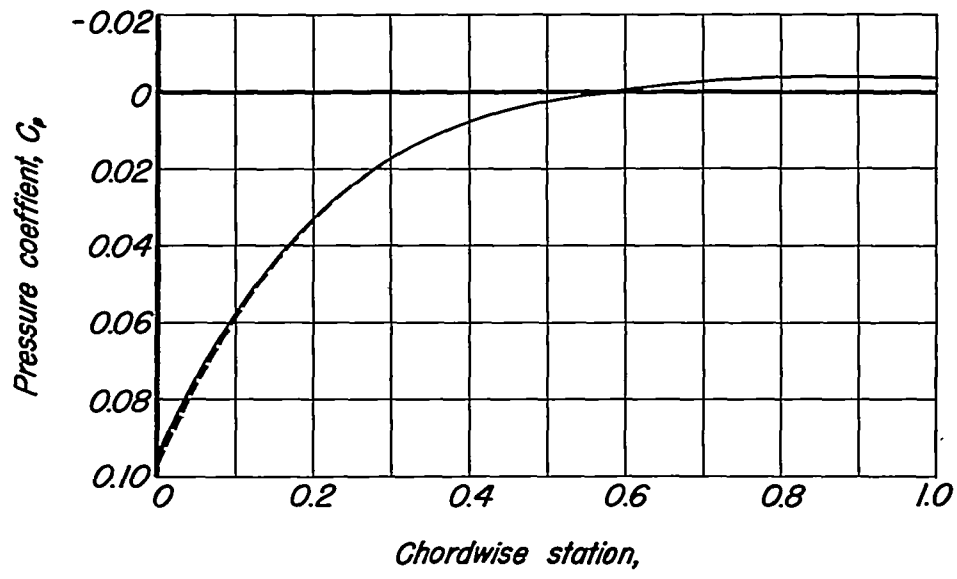

(a) $M_\infty = 20$

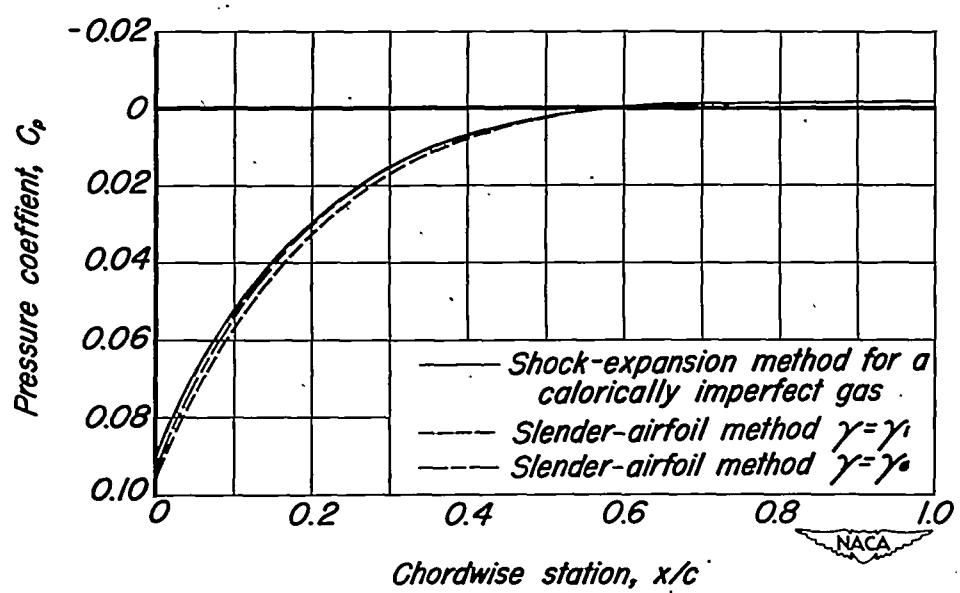

(b) $M_\infty = 30$

Figure 13.— Pressure distribution on 10-percent-thick biconvex airfoil section at $\alpha = 0$ and $T_\infty = 500°R$.

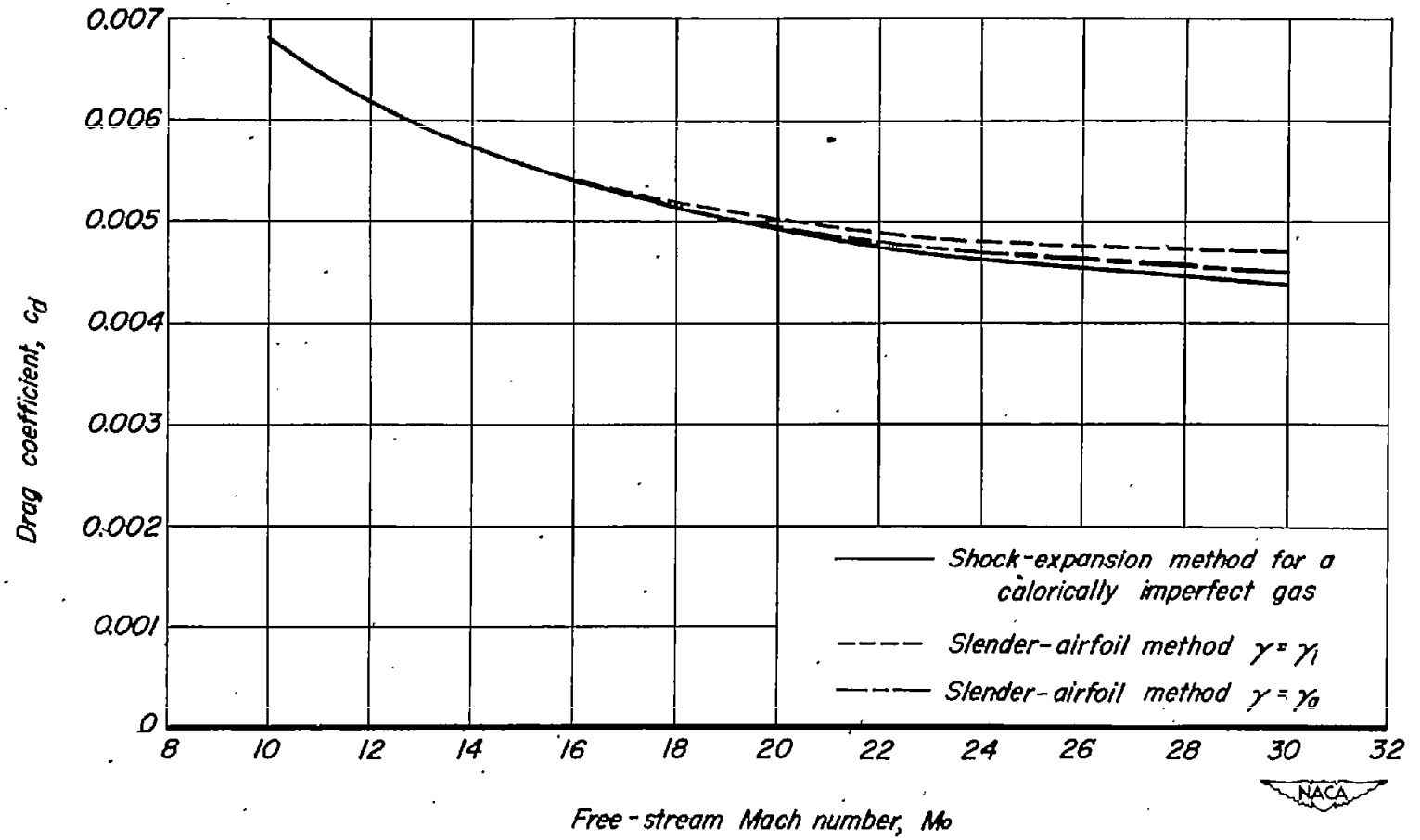

Figure 14.– Variation of drag coefficient with Mach number for 10-percent-thick biconvex airfoil section for $\alpha = 0°$ and $T_0 = 500°R$.

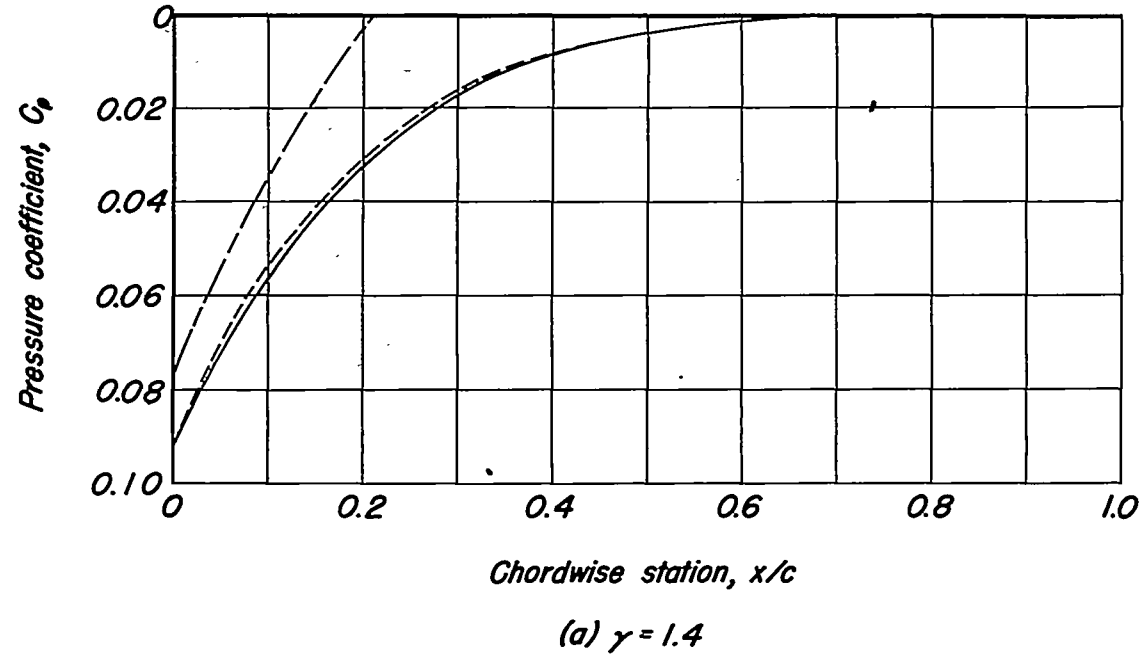

(a) $\gamma = 1.4$

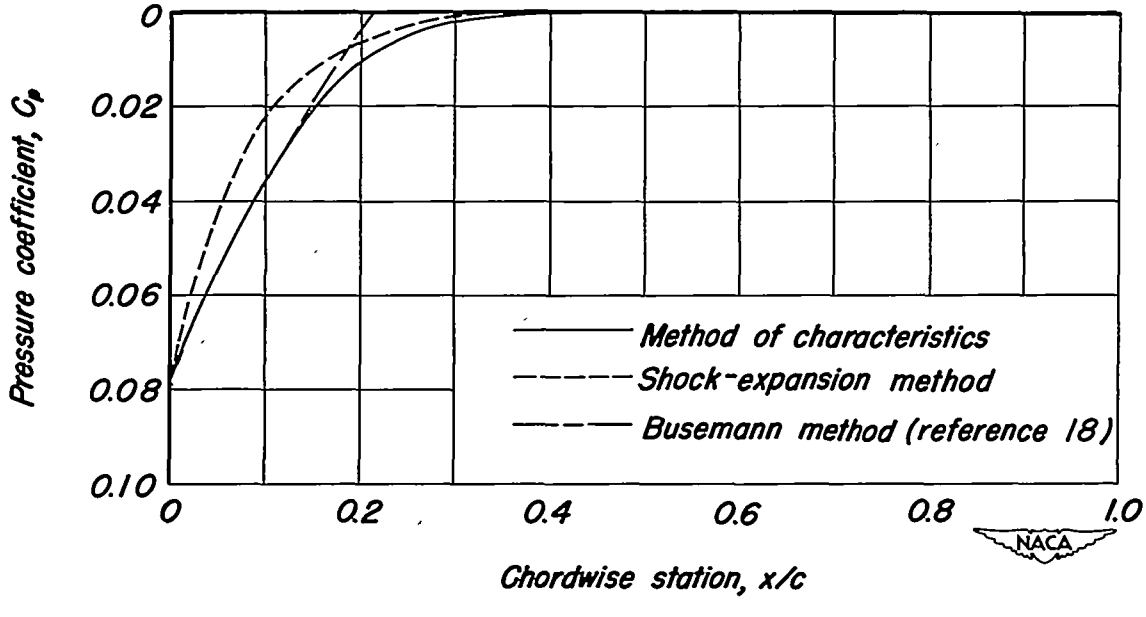

(b) $\gamma = 1.05$

Figure 15. — Pressure distribution on 10-percent-thick biconvex airfoil section at $M_0 = \infty$ and $\alpha = 0°$.

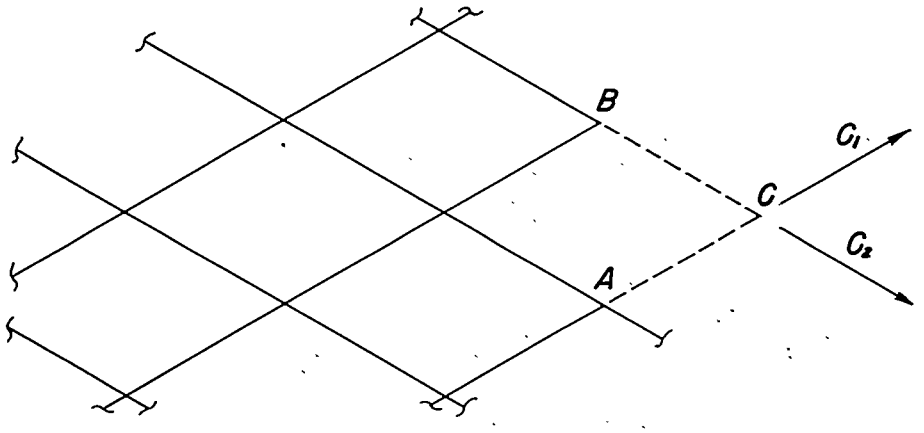

(a) Point in field.

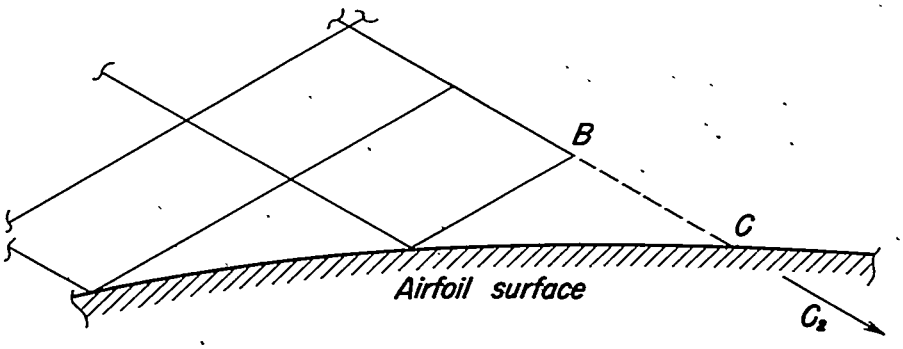

(b) Point on surface.

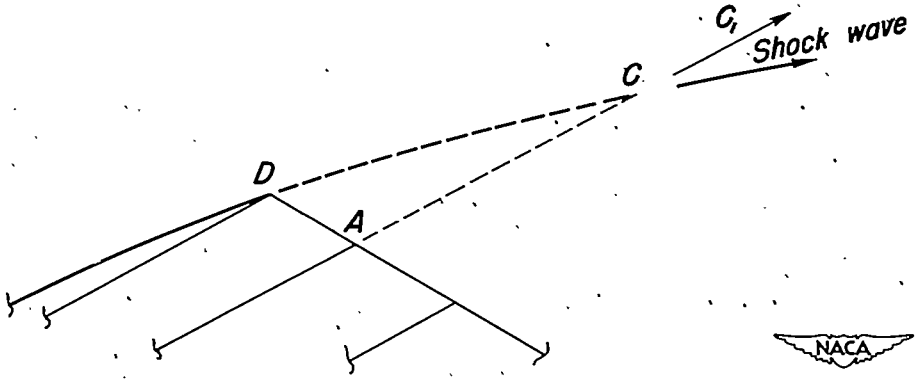

(c) Point on shock wave.

Figure 16.—Diagram of point system in the method of characteristics for the two-dimensional flow of a calorically imperfect gas.

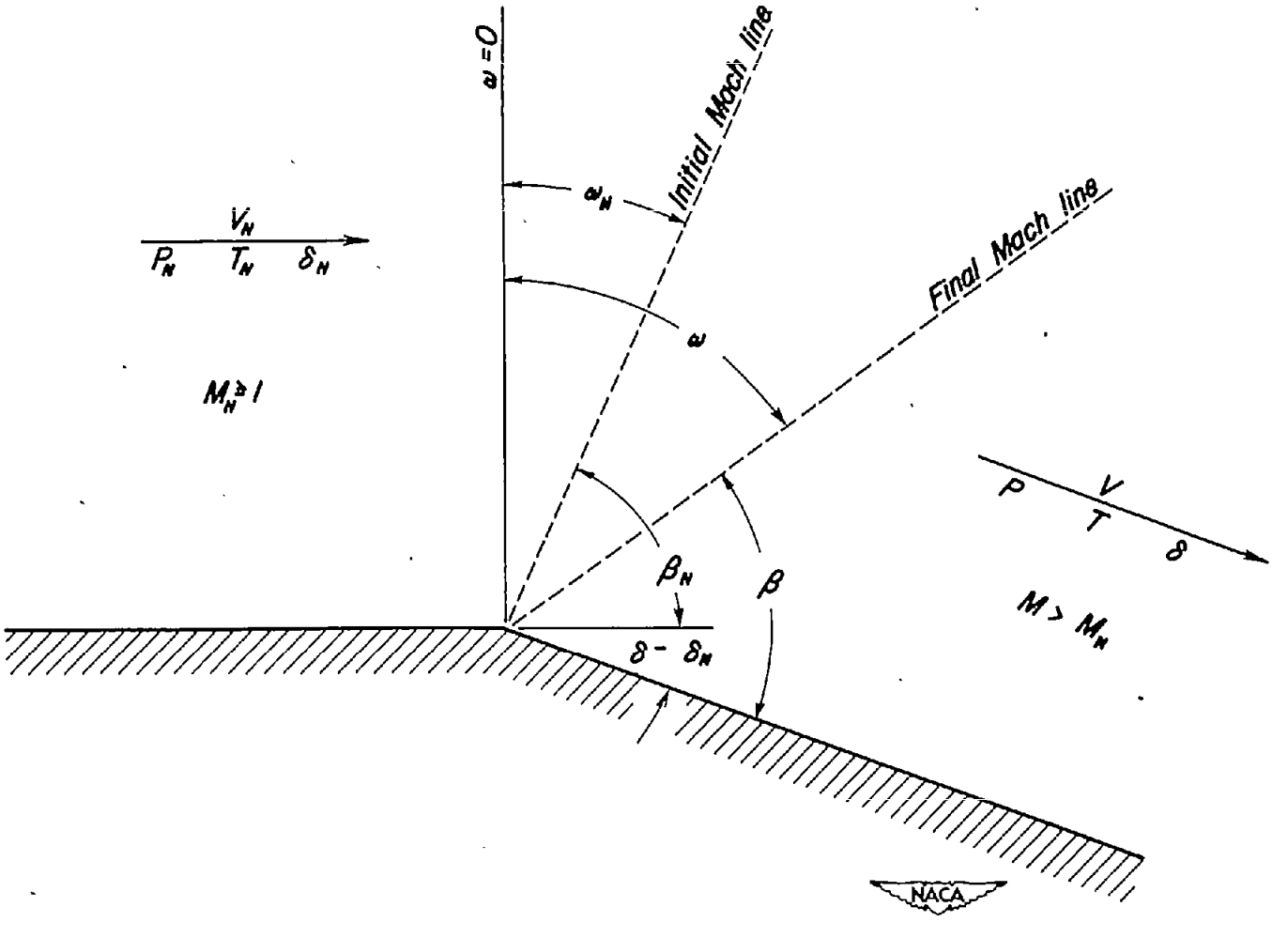

Figure 17.— Schematic diagram of Prandtl—Meyer flow around a corner.

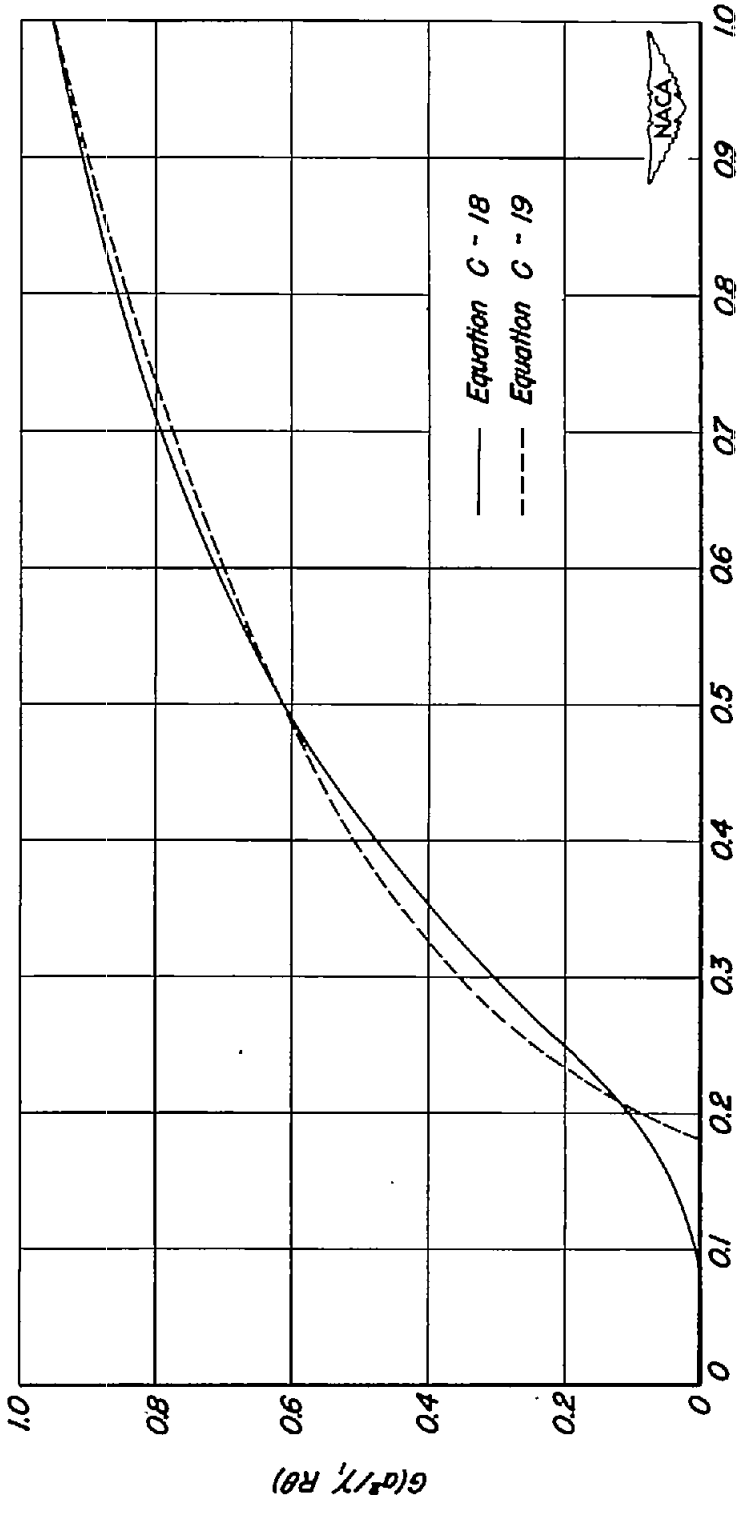

Figure 18. — Accuracy of approximation used in appendix C to obtain solution for Prandtl - Meyer flow of a calorically imperfect gas.

NACA-Langley - 3-3-52 - 1000